Stratigraphy, paleomagnetism, and anisotropy of magnetic susceptibility of the Miocene Stanislaus Group, central Sierra Nevada and Sweetwater Mountains, California and Nevada

Nathan M. King*
Geology Department, California State University, Sacramento, California 95819, USA

John W. Hillhouse
U.S. Geological Survey, 345 Middlefield Road, Menlo Park, California 94025, USA

Sherman Gromme
420 Chaucer Street, Palo Alto, California 94301-2201, USA

Brian P. Hausback
Geology Department, California State University, Sacramento, California 95819, USA

Christopher J. Pluhar
Earth Sciences Department, University of California, Santa Cruz, California 95064-1077, USA

ABSTRACT

Paleomagnetism and anisotropy of magnetic susceptibility (AMS) reveal pyroclastic flow patterns, stratigraphic correlations, and tectonic rotations in the Miocene Stanislaus Group, an extensive volcanic sequence in the central Sierra Nevada, California, and in the Walker Lane of California and Nevada. The Stanislaus Group (Table Mountain Latite, Eureka Valley Tuff, and the Dardanelles Formation) is a useful stratigraphic marker for understanding the post–9-Ma major faulting of the easternmost Sierra Nevada, uplift of the mountain range, and transtensional tectonics within the central Walker Lane. The Table Mountain Latite has a distinctively shallow reversed-polarity direction (I = –26.1°, D = 163.1°, and α_{95} = 2.7°) at sampling sites in the foothills and western slope of the Sierra Nevada. In ascending order, the Eureka Valley Tuff comprises the Tollhouse Flat Member (I = –62.8°, D = 159.9°, α_{95} = 2.6°), By-Day Member (I = 52.4°, D = 8.6°, α_{95} = 7.2°), and Upper Member (I = 27.9°, D = 358.0°, α_{95} = 10.4°). The Dardanelles Formation has normal polarity. From the magnetization directions of the Eureka Valley Tuff in the central Walker Lane north of Mono Lake and in the Anchorite Hills, we infer clockwise, vertical-axis rotations of ~10° to 26° to be a consequence of dextral shear. The AMS results from 19 sites generally show that the Eureka Valley Tuff flowed outward from its proposed source area, the Little Walker Caldera, although several indicators are transverse to radial flow. AMS-derived flow patterns are consistent with mapped channels in the Sierra Nevada and Walker Lane.

Keywords: ash-flow tuff, Miocene, California, paleomagnetism, magnetic anisotropy

INTRODUCTION

The late Miocene Stanislaus Group consists of widespread volcanic units that extend from the western foothills of the Sierra Nevada in California, across the crest of the Sierra Nevada, and into the Basin and Range Province of western Nevada (Fig. 1). Just east of the drainage divide at Sonora Pass, the volcanic succession is very thick and bears proximal features that have been interpreted as being part of a caldera rim. The Little Walker Caldera, which underlies a roughly circular valley in this area, is the proposed source of the Stanislaus Group (Slemmons, 1966; Noble et al., 1974; Priest, 1979). Lava flows and ash-flow tuffs of the Stanislaus Group (Table 1) were deposited in a series of west-draining canyons, such as the Cataract Channel (Ransome, 1898; Lindgren, 1911) in the Sierra Nevada, which may have connected with highlands in western Nevada. Outcrops of the Stanislaus Group (ca. 9.5 Ma) on the western slope of the central Sierra Nevada are remnants of deposits that once choked the Miocene paleovalley system.

Today, the high eastern scarp of the Sierra Nevada separates the western volcanic flows from the proposed caldera source, with the base of the flows now standing 1500 m above the caldera. Whether the high scarp, which formed since 5 Ma, is the product of rapid uplift of the Sierra Nevada (Unruh, 1991; Wakabayashi and Sawyer, 2001) or collapse of a high-standing plateau (Wolfe et al., 1997; Mulch et al., 2006) remains a matter for debate. The paleotopography of the Miocene volcanic rocks and the underlying Eocene gold-bearing gravels is critical to arguments concerning paleoelevation, isostasy, and midcrustal dynamics of the region.

East of the Sierra Nevada, the Stanislaus Group is in the tectonically active, central Walker Lane (Stewart, 1988). Late Cenozoic and contemporary movement of the Pacific plate relative to North America is partially

*Current address: San Francisco Bay Regional Water Quality Control Board, 1515 Clay St., Oakland, CA 94612, USA

Geosphere; December 2007; v. 3; no. 6; p. 646–666; doi: 10.1130/GES00132.1; 16 figures; 6 tables.

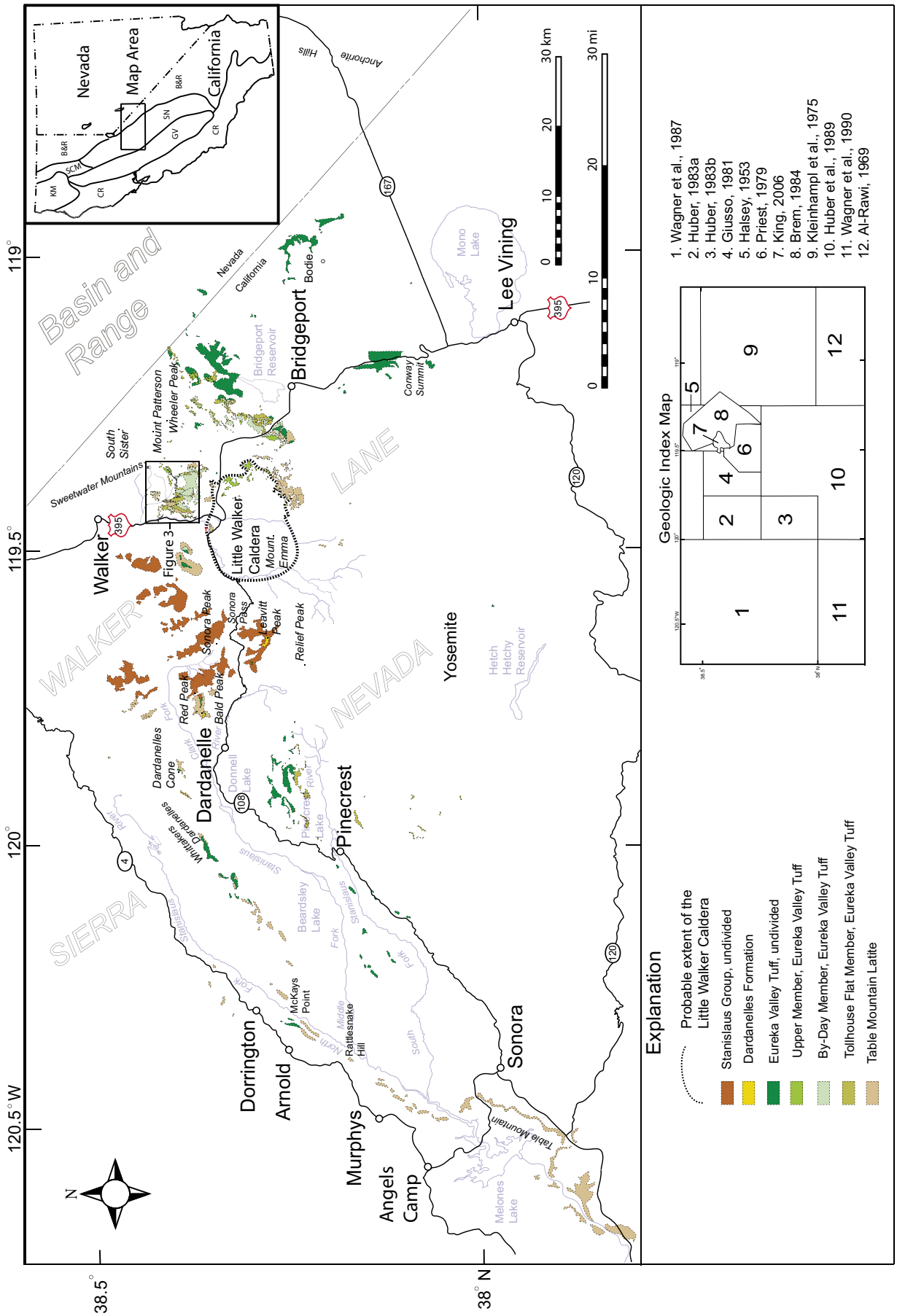

Figure 1. Geologic map and index to mapping of the Stanislaus Group in California and western Nevada. Inset shows physiographic provinces: B&R—Basin and Range; CR—Coast Ranges; GV—Great Valley; KM—Klamath Mountains; SCM—Southern Cascade Mountains; SN—Sierra Nevada.

TABLE 1. EVOLUTION OF STRATIGRAPHIC NOMENCLATURE OF THE STANISLAUS GROUP, CALIFORNIA AND NEVADA

<table>
<tr><td>Ransome (1898)</td><td colspan="2">Slemmons (1966)</td><td colspan="3">Noble et al. (1974); used in this study</td></tr>
<tr><td>Dardanelle Flow</td><td rowspan="4">Stanislaus Formation</td><td>Dardanelles Member</td><td rowspan="4">Stanislaus Group</td><td colspan="2">Dardanelles Formation</td></tr>
<tr><td rowspan="3"></td><td rowspan="3">Eureka Valley Member</td><td rowspan="3">Eureka Valley Tuff</td><td>Upper Member</td></tr>
<tr><td>By-Day Member</td></tr>
<tr><td>Biotite-augite latite</td><td>Tollhouse Flat Member</td></tr>
<tr><td>Table Mountain Flow</td><td>Table Mountain Latite Member</td><td colspan="2">Table Mountain Latite</td></tr>
<tr><td colspan="6">Note: Modified from Noble et al. (1974), in which Tollhouse Flat Member and Table Mountain Latite are equivalent to Ransome's (1898) biotite-augite latite and Table Mountain Flow, respectively.</td></tr>
</table>

accommodated (20%) across the Walker Lane, with the rest of the strain being taken up by the San Andreas fault system (Argus and Gordon, 1991; Hearn and Humphreys, 1998; Atwater and Stock, 1998; Wernicke and Snow, 1998; Thatcher et al., 1999; Bennett et al., 2003; McQuarrie and Wernicke, 2005). Beds of the Stanislaus Group and other late Cenozoic deposits within the Walker Lane are broken and tilted by a complex of strike-slip and normal faults that formed in response to northward movement of the Sierra Nevada block, Basin-and-Range extension, and dextral shear (Stewart, 1988; Faulds et al., 2005; Wesnousky, 2005). Understanding the original distribution of the Stanislaus Group provides important reference datum for reconstructing the regional tectonic history since 9.5 Ma. Therefore, we undertook this study of magnetic properties to provide basic data relevant to the source and regional correlation of the Stanislaus Group.

The primary objective of this study is to investigate patterns of flow in the Miocene volcanic succession by measuring anisotropy of magnetic susceptibility (AMS) of the Eureka Valley Tuff, the most widespread formation of the Stanislaus Group. Microscopic examination of ash-flow tuff has revealed preferred orientation of elongate crystals and glass shards, and this fabric is attributed to laminar flow during end-stage emplacement of ignimbrites (Elston and Smith, 1970; Rhodes and Smith, 1972). AMS has been shown to be an effective proxy for flow fabric in ash-flow tuffs (Ellwood, 1982; Incoronato et al., 1983; Knight et al., 1986; Hillhouse and Wells, 1991; Palmer et al., 1991, 1996; Baer et al., 1997; Palmer and MacDonald, 1999). Ash-flow tuffs typically exhibit an oblate, AMS ellipsoid with a near-vertical minimum axis due to compaction and with a near-horizontal maximum axis parallel to the flow direction. Imbrication of the magnetic foliation plane, defined by orientation of the maximum-intermediate susceptibility plane, indicates the sense of flow. Our strategy was to test the utility of AMS as a flow indicator in well-known channel-filling deposits and, if successful, to apply the method elsewhere to delineate the broader channel system in isolated volcanic remnants. Also, we wanted to test whether the pattern of flow is consistent with a source area centered on the Little Walker Caldera. Establishment of a radial flow pattern outward from the caldera would confirm the proposed source of the Eureka Valley Tuff.

A necessary complement to the AMS study was the measurement of natural remanent magnetization at sites within the Stanislaus Group. Vertical-axis rotation is likely within the tectonically active areas east of the eastern Sierra Nevada escarpment (Cashman and Fontaine, 2000); therefore, it was necessary to account for any rotations in the interpretation of the AMS flow directions. Assuming that upon rapid cooling, a widespread ash-flow tuff will acquire a uniform direction of magnetization, the declination of remanent magnetization preserved in the tuff is a useful indicator of tectonic rotation (Gromme et al., 1972; Young and Brennan, 1974; Wells and Hillhouse, 1989; Palmer et al., 1991). From ash-flow sites on the relatively stable Sierra Nevada block, we established a virtual geomagnetic pole to provide a frame of reference for measuring rotations in the Sweetwater Mountains and nearby Basin-and-Range areas.

The regional magnetostratigraphy of the Stanislaus Group also was determined as part of this paleomagnetic investigation. The principal author collected samples from the Eureka Valley Tuff and Table Mountain Latite, and this collection was combined with material obtained by the U.S. Geological Survey from early studies (1962 and 1963) of the Stanislaus Group. The resultant magnetostratigraphy of the Stanislaus Group is useful for making regional geologic correlations vital to our understanding of the late-Cenozoic uplift of the central Sierra Nevada and the tectonic processes of the Sierra Nevada-Walker Lane transition.

PREVIOUS WORK

The volcanic rocks now known as the Stanislaus Group (Table 1; Noble et al., 1974) have captured the interest of geologists for 150 yr. Trask (1856) and Whitney (1865) were early observers of the "Table Mountain Flow" near Sonora, California. They noted the inverted position of the "basalt" within an older stream channel positioned above the current drainages. Ransome (1898) described the Table Mountain Flow in more detail, defining the stratigraphy as a lower latite (Table Mountain Flow), a middle biotite-augite latite, and an upper latite (Dardanelle flow). The sinuous lava flows of Table Mountain filled a paleovalley known as the Cataract Channel (Ransome, 1898; Slemmons, 1953), and the flows probably originated from dikes between Sonora Pass and Bald Peak near the Sierra Nevada divide (Slemmons, 1953). East of the divide in the Sweetwater Mountains, the Table Mountain Latite of Noble et al. (1974) possibly originated from both the dikes and the Little Walker Caldera (Priest, 1979).

Johnson (1951), Halsey (1953), Slemmons (1953, 1966), Gilbert et al. (1968), Chesterman (1968), and Al-Rawi (1969) mapped ash-flow tuffs in the southern Sweetwater Mountains, the Bodie Hills, and nearby areas. They recognized the similarities of these units to tuffs, including the biotite-augite latite of Ransome (1898), in the Sierra Nevada. Slemmons (1966) named these ash-flow tuffs for Eureka Valley at the foot of Bald Peak, 10 km west of Sonora Pass (Fig. 1). Noble et al. (1969) and Priest (1979) proposed that the source of the tuffs is the Little Walker Caldera, based on lag-fall deposits that crop out on its eastern margin, occurrence of blocks of Eureka Valley Tuff within lacustrine tuffs that they interpreted to be caldera rim landslide deposits in an intra-caldera lake, and the presence of an elliptical depression. Noble et al. (1974) defined the current stratigraphic nomenclature of the Stanislaus Group (Table 1). Brem (1977) studied the regional

volcanic stratigraphy in his doctoral thesis and later produced an excellent geologic map of the Sweetwater roadless area (Brem, 1984).

Early attempts to date the various formations of the Stanislaus Group were summarized by Noble et al. (1974), who reported potassium-argon ages of 9.0 ± 0.2 Ma (Table Mountain Latite), 8.8 ± 0.2 Ma to 10.7 Ma (Tollhouse Flat Member, Eureka Valley Tuff), and 9.9 ± 0.4 Ma to 10.0 ± 0.3 Ma (Upper Member, Eureka Valley Tuff) largely based on the work of Dalrymple (1963, 1964) and Dalrymple et al. (1967). In some cases, the range of age determinations violated stratigraphic position, and Noble et al. (1974) gave a preferred age of 9.5 Ma (ca. 9.7 Ma, adjusted for modern decay constants) for the Eureka Valley Tuff. The first paleomagnetic polarity determinations from the Table Mountain Latite (W33), Tollhouse Flat Member (W29, W23, W24), and Upper Member (W25) were given by Dalrymple et al. (1967). Al-Rawi (1969) used a portable, flux-gate magnetometer to measure the polarity of remanent magnetization of the Eureka Valley Tuff (Tollhouse Flat Member reversed magnetic polarity; By-Day and Upper member normal magnetic polarities), and he demonstrated the value of paleomagnetism to distinguish these ash flows from one another.

REGIONAL GEOLOGIC SETTING OF THE STANISLAUS GROUP

The stratigraphy of the central Sierra Nevada as described by Slemmons (1966) includes Cretaceous granitic plutons of the Sierra Nevada batholith that are nonconformably overlain by Tertiary rhyolitic to andesitic volcanic and sedimentary rocks. From bottom to top, these Tertiary rocks include Eocene auriferous gravels, the Oligocene-Miocene rhyolitic Valley Springs Formation (Piper et al., 1939), the Miocene andesitic Relief Peak Formation (Slemmons, 1966), the Miocene Stanislaus Group (Ransome, 1898; Slemmons, 1966; Noble et al., 1974), and the andesitic Disaster Peak Formation (Slemmons, 1966).

Formations of the Stanislaus Group crop out in a 150-km–long, east-trending band from the foothills of the Sierra Nevada to a few kilometers into Nevada (Fig. 1). The maximum north-south width is ~60 km near longitude 120º, west of Sonora Pass. The Table Mountain Latite and Tollhouse Flat Member of the Eureka Valley Tuff are the most widespread units of the Stanislaus Group. Nowhere is the complete section of the Stanislaus Group present (Table 2).

GEOCHEMISTRY OF THE STANISLAUS GROUP

Geochemical analyses were completed at Washington State University using X-ray fluorescence (XRF) and inductively coupled plasma (ICP) mass spectrometry. Major- and trace- element analyses of our samples from the Stanislaus Group are included in Appendix A[1]. For completeness, the appendix also includes summary tables of major-element compositions from samples analyzed by Ransome (1898), Noble et al. (1974), Priest (1979), and Brem (1977). The samples collected during the current study consisted of juvenile material from the Eureka Valley Tuff and whole-rock samples from the Table Mountain Latite and Rhyolite of the Sweetwater Mountains of Brem (1984). The Eureka Valley Tuff samples were collected from fiamme in the Tollhouse Flat and By-Day Members and from pumice lapilli in the Upper Member. Eureka Valley Tuff Upper Member samples analyzed by Brem (1977) were whole-rock samples. Additionally, compositions of Tollhouse Flat Member samples reported by Ransome (1898) most likely were also whole-rock samples. The remaining samples collected by Brem, Noble, and Priest were collected from juvenile material.

The Stanislaus Group consists of primarily potassic to highly potassic lava flows and ash- flow tuffs that range from basaltic trachyandesite to trachyte (Fig. 2), according to the IUGS (International Union of the Geological Sciences) classification (Le Bas et al., 1986). Chemical compositions of the Table Mountain Latite are bimodal with groups of potassic basaltic trachyandesite and trachyte lava flows. Priest (1979) attributed the lower Table Mountain mafic flows to the dikes near Sonora Pass and possibly from the Little Walker Caldera; the much thinner and less voluminous upper silicic flows, which only crop out several kilometers around the Little Walker Caldera, were attributed to the Little Walker Caldera. The Eureka Valley Tuff is unwelded to densely welded, lapilli ash-flow tuffs that range in composition from trachyte to dacite. The Dardanelles Formation consists of trachyandesite lava flows (Slemmons, 1966).

GEOLOGIC MAP AND LOCAL STRATIGRAPHY: SWEETWATER MOUNTAINS

A detailed geologic map (Figs. 3 and 4; King, 2006) provides context for the Eureka Valley Tuff reference section at Tollhouse Flat, California. Noble et al. (1974) added

TABLE 2. COLUMNAR SECTIONS OF THE STANISLAUS GROUP, CALIFORNIA AND NEVADA

Locations						
Rattlesnake Hill	McKays Point	Whittakers Dardanelles	Bald Peak	Sonora Pass	EVT Reference Section, Sweetwater Mountains	Bodie and Mono Lake
		Dardanelles Formation	Dardanelles Formation	Dardanelles Formation		
					Upper Member, EVT	Upper Member, EVT
					By-Day Member, EVT	
	Tollhouse Flat Member, EVT	Tollhouse Flat Member, EVT	Tollhouse Flat Member, EVT	Tollhouse Flat Member, EVT	Tollhouse Flat Member, EVT	Tollhouse Flat Member, EVT
Table Mountain Latite	Table Mountain Latite	Table Mountain Latite		Table Mountain Latite	Table Mountain Latite	

Note: See Figure 1 for locations. Sonora Pass section modified from Slemmons (1966). EVT—Eureka Valley Tuff.

[1]If you are viewing the PDF of this paper or reading it offline, please visit http://dx.doi.org/10.1130/GES00132.S1 or the full-text article on www.gsajournals.org to view Appendix A.

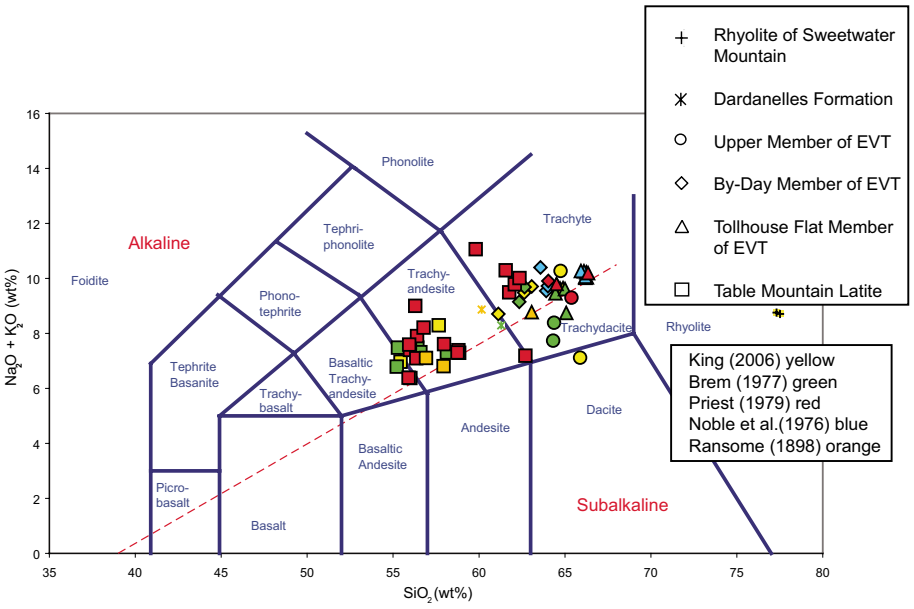

Figure 2. Total alkali versus silica diagram (Le Bas et al., 1986) of the Stanislaus Group. Analytical results are from Appendix A (see footnote 1). Alkaline/subalkaline dividing line (red dashed line) of Irvine and Baragar (1971) is included for reference. EVT—Eureka Valley Tuff.

this reference section, because the type locality of the Eureka Valley Tuff on Bald Peak near Sonora Pass (Slemmons, 1966) is remote, and it does not include all of the members of the formation. The Eureka Valley Tuff and the Table Mountain Latite are present in the map area (Fig. 3), but the Dardanelles Formation is not found there.

Detailed Stratigraphy at the Eureka Valley Tuff Reference Section

As measured at Tollhouse Flat, the reference section includes ~28 m of Table Mountain Latite overlain by 185 m of the Eureka Valley Tuff (Fig. 5). The base of the Table Mountain Latite is not exposed in the measured section. The top of the reference section is truncated by a normal fault. The Eureka Valley Tuff dips ~35° to the north at this location (Fig. 6).

Table Mountain Latite

At the reference section, the Table Mountain Latite consists of (from bottom to top) volcaniclastic breccia, gray scoriaceous trachyandesite lava, and cross-stratified, red-tan volcaniclastic sandstone. This volcaniclastic breccia can be distinguished from andesite lahar deposits of Relief Peak Formation by lack of hornblende phenocrysts within the Table Mountain Latite.

Tollhouse Flat Member of the Eureka Valley Tuff

The Tollhouse Flat Member is welded, devitrified, biotite lithic lapilli ash-flow tuff composed of at least two ash-flow units. This member is cliff forming and shows weak, columnar jointing. A distinctive feature of the Tollhouse Flat Member is ubiquitous biotite phenocrysts. The basal contact is a scoured surface on the Table Mountain Latite. The upper contact of the Tollhouse Flat member is an eroded surface covered by blue-gray sandstone.

By-Day Member of the Eureka Valley Tuff

The By-Day Member is a eutaxitic, lithic lapilli ash-flow tuff consisting of three simple cooling units with alternating partially welded and densely welded zones (vitrophyres). These cooling units give the By-Day Member a distinctive layered appearance in comparison with the underlying Tollhouse Flat Member. The By-Day Member is distinguishable from the Upper and Tollhouse Flat Members by the lack of biotite phenocrysts within the pumice lapilli and fiamme (Halsey, 1953; Noble et al., 1974; Brem, 1984). Rare biotite phenocrysts are present within the groundmass, but are probably xenocrysts. The welded zones have weak, columnar jointing and are cliff forming. The basal contact is a sharp surface scoured into the underlying blue-gray sandstone unit. The upper contact with the overlying Upper Member is covered by colluvium.

Upper Member of the Eureka Valley Tuff

The Upper Member of the Eureka Valley Tuff is only partly exposed at the reference section and within the drainage to the east (Fig. 4). The Upper Member contains at least six biotite lapilli ash-flows ranging from unwelded tuff to densely welded vitrophyres. These ash-flows are (bottom to top) a white unwelded tuff, a tan unwelded tuff, two densely welded tuffs with vitrophyres, an upper, tan unwelded tuff and an upper, white unwelded tuff. The thicknesses of the two upper unwelded tuffs were not measured because of poor exposure. The unwelded tuffs in the Upper Member are easily eroded, form gentle slopes, and are characterized by conspicuous white and tan hoodoos (weathered pinnacles).

MAGNETIC INVESTIGATION

Field Methods and Specimen Preparation

Samples for magnetic studies were collected from 36 localities in the Stanislaus Group (Fig. 7). In 1962, Sherman Gromme collected oriented block samples at 14 sites (WD2–WD10, BP3, BP7, JR, MK13, and DM1–DM11), and drilled oriented cores in the field at three sites (MK1, PW26, and RH3). All of these samples were collected from near-horizontal beds in the central Sierra Nevada. Effects of local magnetic anomalies were checked with a small vertical-component magnetic balance. The magnetic azimuths were corrected by backsighting to a second compass only at one site (RH3), where the magnetizations from lightning strikes were strong. Oriented cores were drilled from the block samples using a drill press at the laboratory. In 1963, three sites in the southeast outcrop area (3V129, 3V138, and 3V156) were sampled by Allan Cox (U.S. Geological Survey), who drilled cores in the field. These cores were oriented with a magnetic compass. The azimuths were checked for local magnetic effects by backsighting to landmarks.

Christopher Pluhar drilled core samples from the Table Mountain Latite at Rawhide Road (RR), Murphys Cliff (MC), and Lower Griswold Creek (LG) in 1996. These samples were oriented with a magnetic compass and clinometer; declination corrections were measured by either sun compass or backsighting methods. No bedding attitude corrections were suggested by field relations at these three localities, and, thus, none have been applied.

The remaining samples (all with LW prefixes) were collected by the principal author during the current study using portable

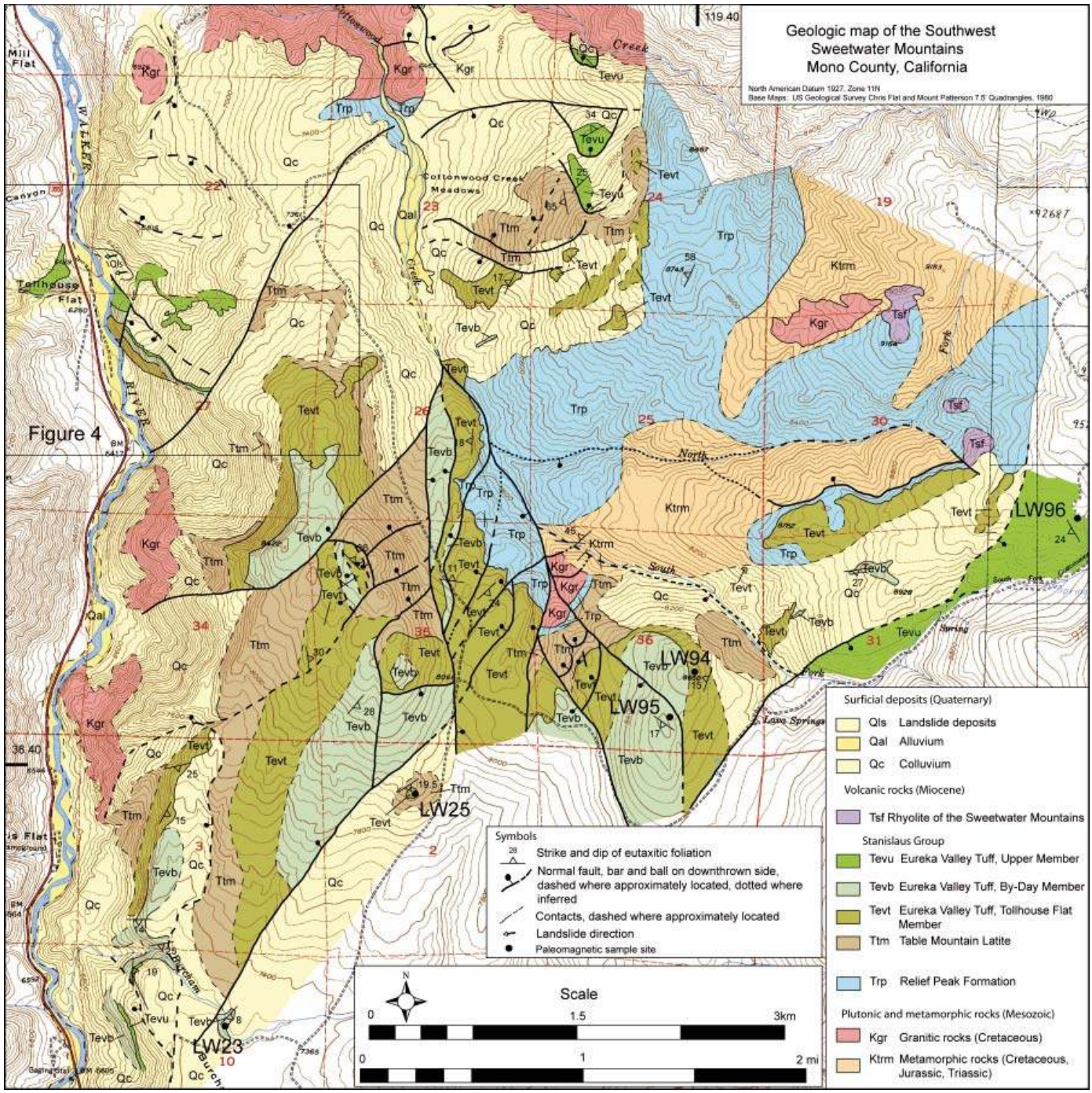

Figure 3. Geologic map of part of the Sweetwater Mountains, California, from King (2006). The mapped area is within the Chris Flat and Mount Patterson quadrangles (1:24,000).

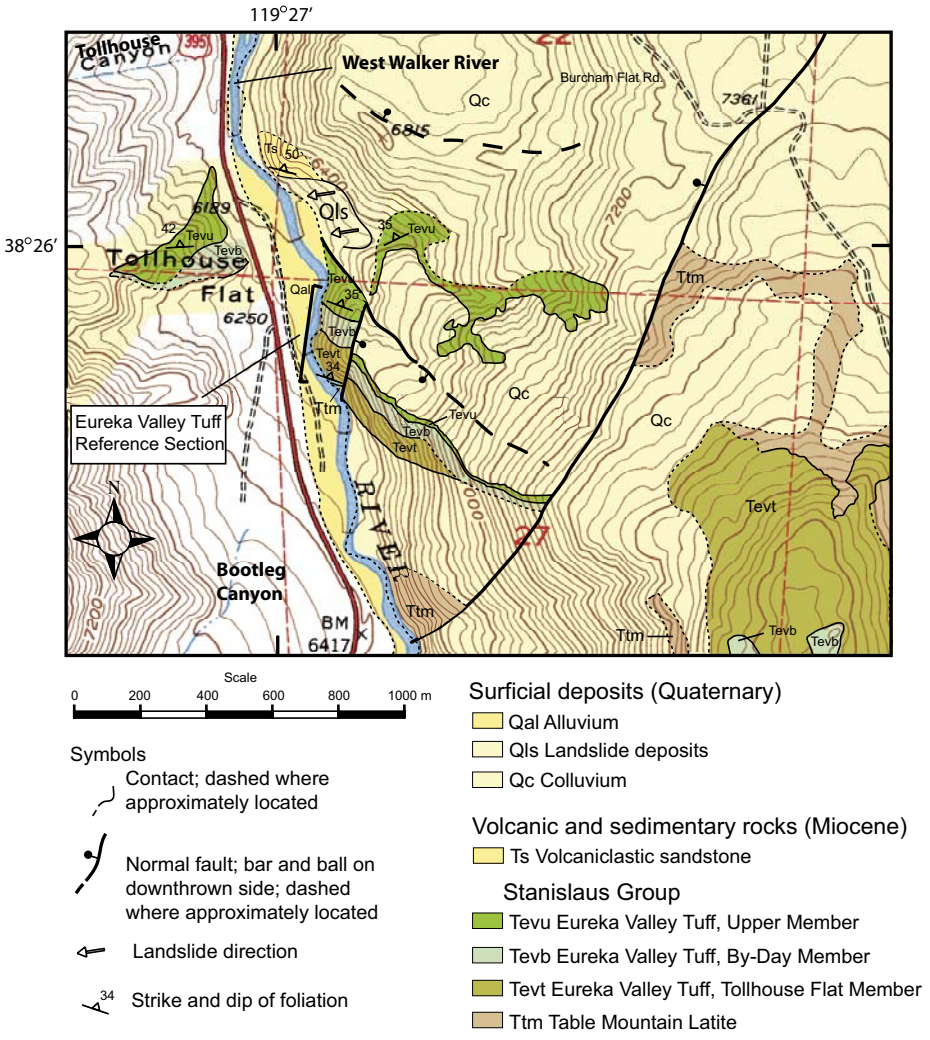

Figure 4. Geologic map showing reference section of the Eureka Valley Tuff at Tollhouse Flat, California. Excerpted from King (2006).

drilling equipment. These cores were oriented with a magnetic compass (LW23–LW92) or a sun compass (LW93–LW98). Five to 13 cores were collected from each site. The sampling site locations were determined using a handheld GPS (Global Positioning System) unit. Each oriented core (sample) was cut into one to three specimens ~2.54 cm long. Attitudes of flattened pumice clasts (fiamme) were averaged together to obtain tilt corrections for each site in the Eureka Valley Tuff.

Laboratory Methods: Remanent Magnetization

The remanent magnetization measurements of the Cox collection were conducted with a spinner magnetometer at the U.S. Geological Survey (USGS) Rock Magnetism Laboratory during 1963 to 1965. Alternating-field (AF) demagnetizations were done at 10 or 20 mT with a 60-Hz coil and three-axis tumbling sample holder. Dalrymple et al. (1967) reported K-Ar ages and polarity determinations, but not specific directions of magnetization, from 3V129 (W23), 3V138 (W24), and 3V156 (W25). Preliminary measurements of Gromme's collection were made in 1965 and 1966 in Berkeley and Menlo Park. Dalrymple et al. (1967) reported polarity determinations and K-Ar ages from RH3 (W33), BP3 (W32), and BP7 (W29). The principal author completed demagnetization treatments of the entire collection at the USGS laboratory in Menlo Park, California. The remanent magnetization measurements performed in this study were conducted with a three-axis cryogenic magnetometer. Progressive step AF demagnetization to 100 mT was done in a shielded coil driven at 400 Hz with the specimen held in a reciprocating, two-axis tumbler. Thermal demagnetization was applied to one specimen from LW95 (By-Day Member), LW97 (Tollhouse Flat Member), and LW98 (Table Mountain Latite) to examine unblocking-temperature distributions. Heating was performed in air in a magnetically shielded furnace (internal field <10 nT).

The remanent magnetization measurements resulting from the AF demagnetization treatments were analyzed with orthogonal vector component diagrams (Zijderveld, 1967). The characteristic magnetization (ChRM) direction, defined by demagnetization steps following a linear path to the origin of the orthogonal diagram, was calculated by principal component analysis (Kirschvink, 1980; Cogné, 2003). If a stable magnetization direction was not achieved, the magnetization of that specimen was not used in the directional analysis. At the lower Griswold Creek site, some samples were affected by strong secondary magnetization (presumably a lightning effect) and did not reach stable magnetizations, but these samples described great circle paths that converged on the cluster of ChRM's from other samples from that locality. Thus, these great circle analyses and ChRM's were combined to yield the lower Griswold Creek locality mean (McFadden and McElhinny, 1988; Cogné, 2003).

The ChRM directions of the specimens were averaged together to produce site-mean directions. Fisher (1953) statistics were used to calculate cones of 95% confidence (α_{95}) about the mean magnetization directions and the concentration parameter (k) for each site. The similarity test of McFadden and Lowes (1981) was used to determine the probability that two site means were indistinguishable. For the analysis of rotations, each specimen direction was transformed to a virtual geomagnetic pole (VGP) for calculation of the site-mean VGP and A_{95} confidence circle.

Paleomagnetic Results

Alternating-field demagnetization greater than 50 mT isolated characteristic magnetizations in all but a few specimens; therefore, the magnetization directions were typically calculated from the 60–100 mT steps (Fig. 8). Comparison of the AF and thermal demagnetization diagrams from a small number of companion specimens shows that the two methods produced nearly identical directions of magnetization in the three specimens tested. Maximum unblocking temperatures of the characteristic magnetization varied from

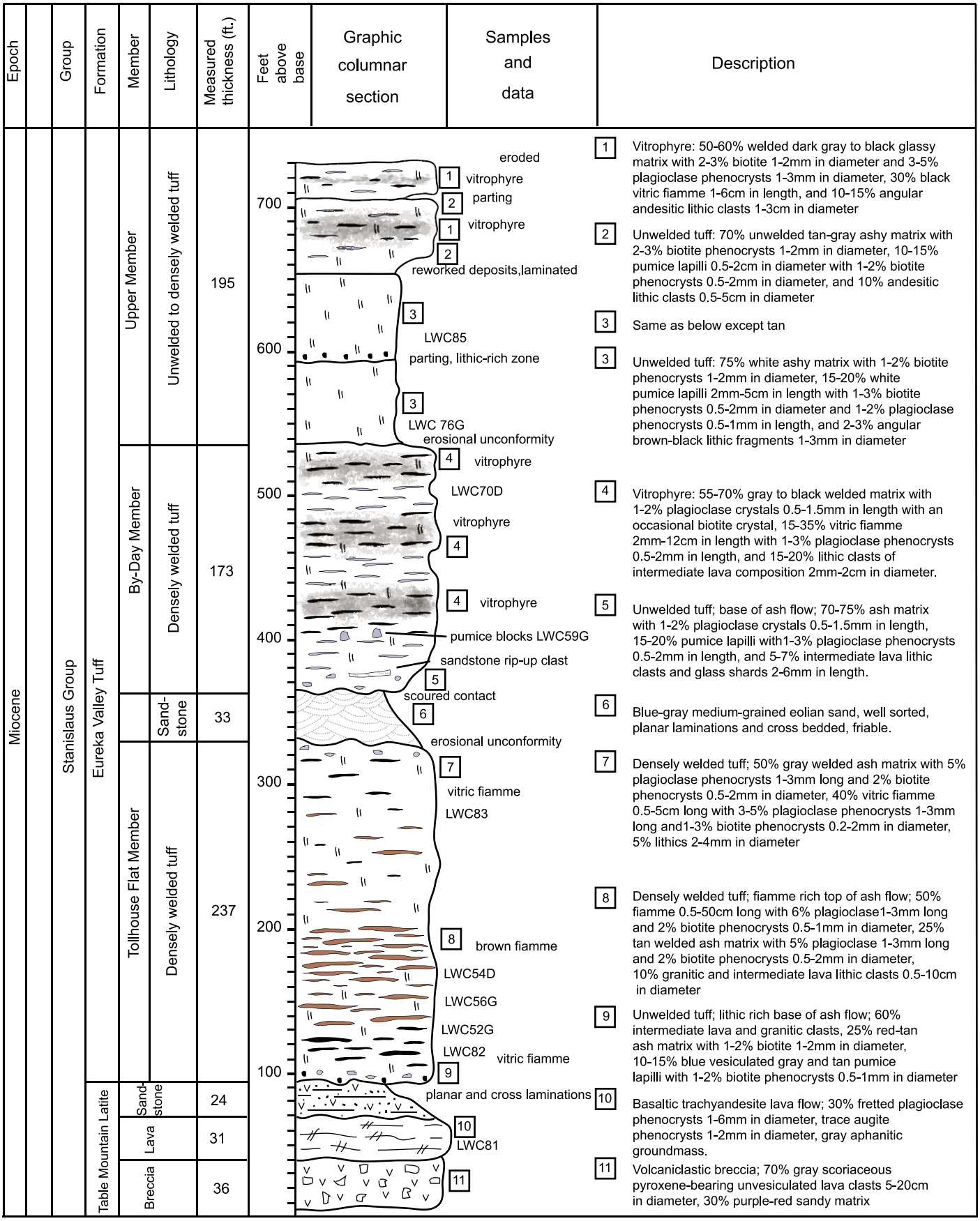

Figure 5. Stratigraphic column with description of the Stanislaus Group at the reference section, Tollhouse Flat, California.

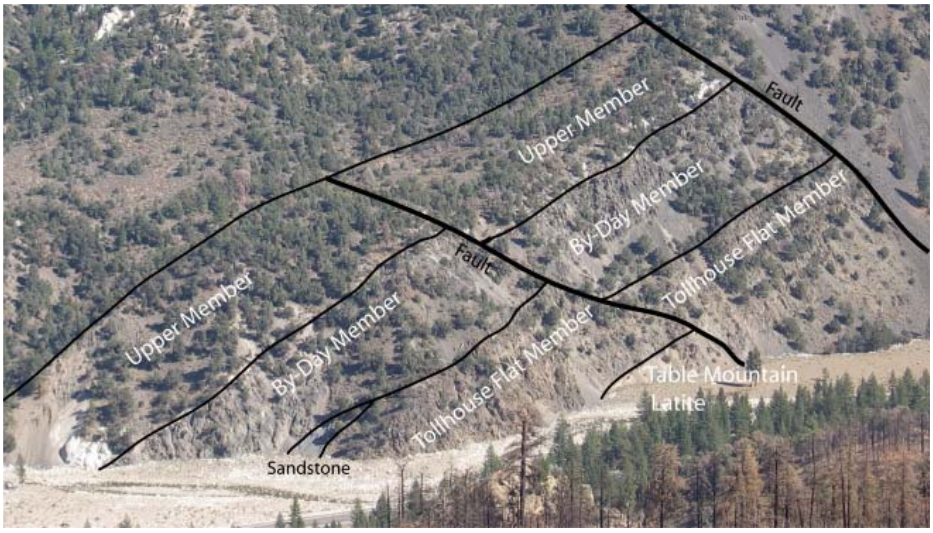

Figure 6. Photograph of the Eureka Valley Tuff reference section. View is eastward with West Walker River and Highway 395 in the foreground. Width of view is ~800 m.

620 °C (Table Mountain Latite and Tollhouse Flat Member) to 570 °C (By-Day Member).

Although some sites initially gave highly scattered remanence directions, presumably due to lightning, the AF treatments were very effective in reducing the scatter. The largest α_{95} is 13.8°, and about two-thirds of the α_{95}'s are less than 5° (Tables 3 and 4). Poor demagnetization results led to rejection of some data from three sites (RH3, PW26, and LW98). Two sites in the Tollhouse Flat Member, LW90 and LW91, gave results that raised questions about the accuracy of some bedding tilt corrections that were measured from fiamme foliations. LW90 and LW91 are located near Pinecrest in the Sierra Nevada, where the volcanic deposits appear to be flat-lying tabular bodies. However, the fiamme foliations suggest tilt up to 17°. Applying the tilt corrections increased the angular difference between remanence directions from LW90 and LW91 as compared to the uncorrected results (24.4°: corrected versus 8.2°: no tilt correction). In this case, we concluded that the fiamme are not a reliable indicator of paleohorizontal bedding, and instead, may reflect the channel topography at the time of deposition. We assumed no appreciable tilt for sites LW90 and LW91, which is consistent with our treatment of all other Stanislaus Group sites in the Sierra Nevada. For sites east of the Sierran crest, where there is significant faulting and tilting, we found that the fiamme-based tilt corrections reduced the spread in inclination by 5° to 15° for all members of the Eureka Valley Tuff with the single exception of LW94. Despite the realization that fiamme foliation is sometimes an inaccurate indicator of paleohorizontal topography, we concluded that the foliation was the best option for making tilt corrections where bedding contacts were poorly exposed in the Sweetwater Mountains. Therefore, we applied the fiamme-based bedding corrections in further analysis of the data from all eastern sites.

The formations and members of the Stanislaus Group are easily distinguished from one another by their magnetic inclinations (Fig. 9). The Table Mountain Latite has an unusual reversed-polarity inclination, which is significantly shallower than the axial dipole field. The overlying Tollhouse Flat Member also has reversed-polarity magnetization, but with a much steeper inclination compared to the Table Mountain Latite direction. A polarity transition occurs between the Tollhouse Flat and the By-Day Members of the Eureka Valley Tuff. The Upper and By-Day Members of the Eureka Valley Tuff have normal polarity directions, with the Upper Member having a distinctive shallow inclination. The overlying Dardanelles Formation has a direction that is similar to the axial dipole and the magnetization direction of the By-Day Member, although the units are easily distinguished on the basis of lithology.

On the western slope of the Sierra Nevada, the Table Mountain Latite appears to be a single-flow unit with a consistent and unusual direction of remanent magnetization as measured from Whittakers Dardanelles westward to the flow terminus at Knight's Ferry (LW98). However, near Sonora Pass, latite flows that have been correlated with the type Table Mountain Latite (Slemmons, 1953, 1966) appear to record a more complex magnetization history. Sites DM 1–11 south of Sonora Pass and near Leavitt Peak span a normal-to-reversed polarity transition in a thick sequence of latite flows that flank the west side of the Little Walker Caldera (Fig. 10). Therefore, it is likely that only one of the many flows that comprise the Table Mountain Latite advanced west of Dardanelles Cone (Fig. 1).

Isothermal Remanent Magnetization (IRM)

We selected seven representative specimens from the Table Mountain Latite and Eureka Valley Tuff for strong-field, IRM-acquisition experiments. Mini-cores (~0.5 g) were magnetized in progressively higher DC (Direct Current) fields to 0.7 Tesla, and the resultant remanent magnetizations were measured. The IRM curves (Fig. 11) are typical of titanomagnetite-bearing rocks, which commonly exhibit IRM saturation above 0.2 Tesla. However, the samples from the Table Mountain Latite show a distinctive inflection in the curve at applied fields of 0.2–0.5 Tesla. We interpret the inflection as evidence that two types of magnetic minerals occur within the latite—titanomagnetite plus a high-coercivity mineral such as titanohematite. Presence of titanohematite is consistent with the high-blocking temperature (620 °C; O'Reilly, 1984) shown by thermal demagnetization of the Table Mountain Latite. As indicated by the back-field part of the IRM curve, the Table Mountain Latite has relatively low coercivity of IRM (0.02 Tesla). This observation is consistent with the latite containing a high proportion of coarse-grained titanomagnetite.

Anisotropy of Magnetic Susceptibility Laboratory Methods

We measured anisotropy of magnetic susceptibility (AMS) of nearly all specimens (excluding RR, MC, and LG) with a Sapphire SI-2 digital susceptibility meter. The meter has a practical sensitivity of 2×10^{-6} SI (International System of Units) (standard deviation of measurements with sample chamber empty). Each specimen was measured in six positions, with a repetition at each position, to solve for the AMS tensor. Specimens were measured for AMS before and after alternating-field demagnetization to assess whether the initial magnetic state affected the AMS results. Some specimens from the Cox and Gromme collections had been demagnetized previously; therefore, AMS could not be measured for the natural state. The rationale for this procedure is based on the observations of Palmer et al. (1996) on the effect of strong-field magnetization on the AMS fabric of the Bishop

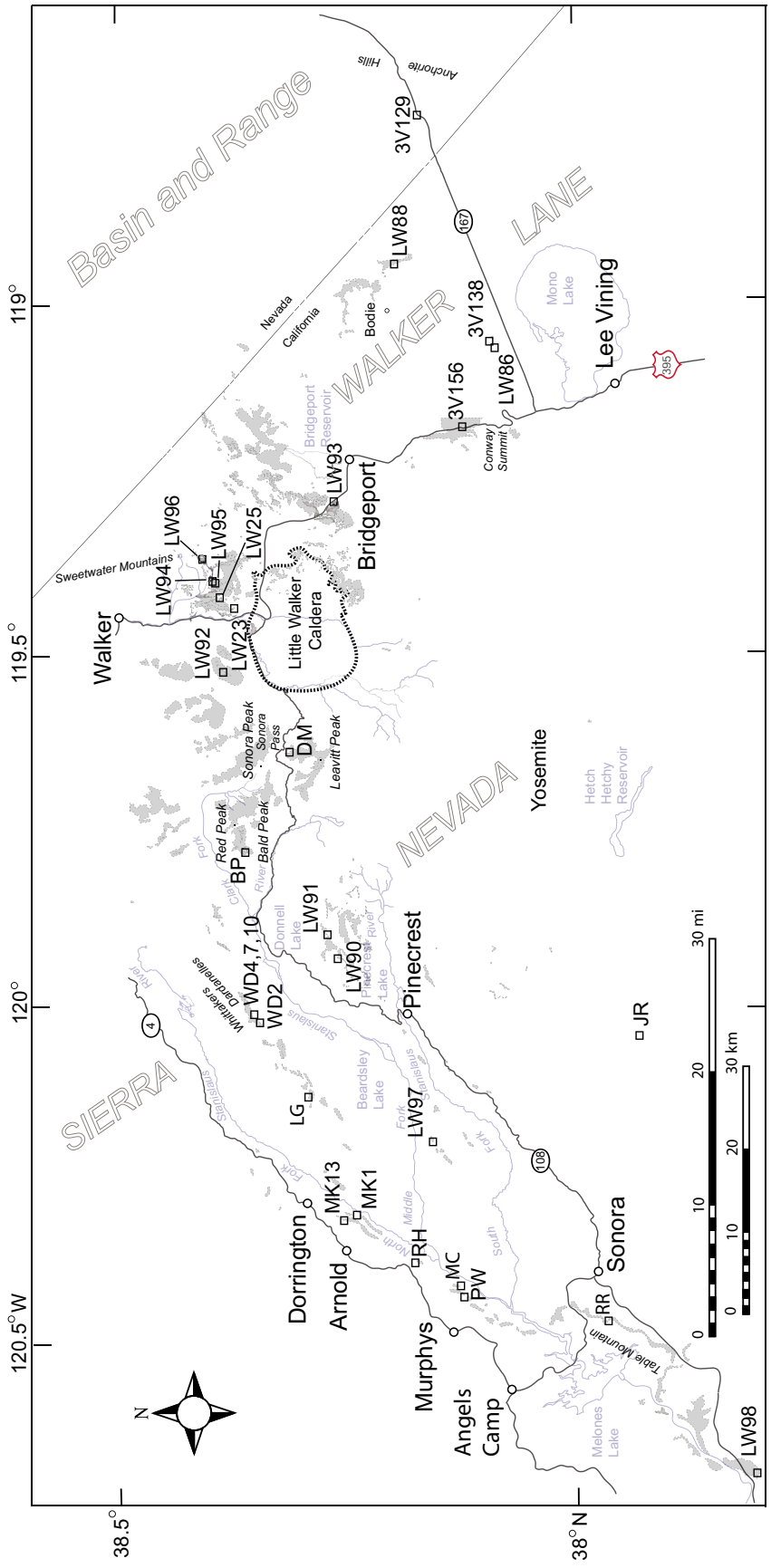

Figure 7. Sites sampled for paleomagnetism in the Stanislaus Group. Site designations are keyed to Table 3. Undifferentiated Stanislaus Group is denoted by stippled pattern.

Tuff. They cautioned that the saturating magnetic field from a lightning strike can greatly change the AMS ellipsoid.

We used the Hext-Jelinek (Hext, 1963; Jelinek, 1978; Lienert, 1991) method to calculate the mean of the specimen principal AMS axes for each site. The method gives 95% confidence ellipses for the three principal axes of the mean susceptibility ellipsoid. After inspecting the site AMS results on a stereogram, we discarded specimen AMS results that plotted far from the site mean confidence ellipses and recalculated the means and confidence limits. A technique similar to this was employed by Le Pennec et al. (1998).

Anisotropy of Magnetic Susceptibility Results

All useful results presented are from specimens collected from the Eureka Valley Tuff (Fig. 12A), which displayed lineated and foliated magnetic fabrics typical of ash-flow tuffs (Incoronato et al., 1983; Hillhouse and Wells, 1991; Le Pennec et al., 1998). The inclinations of the tilt-corrected mean K_{max} and K_{int} axes are near horizontal (plunge generally less than 10º), while the mean K_{min} axes are mainly within 20° of vertical (Table 5). The major 95% confidence ellipses of the K_{max} and K_{int} axes show greater angular dispersion averaging 30°, which is generally twice as wide as the better grouped K_{min} axes. Four of the 19 sites sampled in the Eureka Valley Tuff gave poorly defined K_{max} directions (major 95% confidence limit ≥45°), which are insufficient to constrain flow directions (Fig. 12B).

Specimen susceptibilities are generally 10^{-2} SI, and the meter is capable of measuring 1% anisotropy of these specimens at a signal-to-noise ratio of 50:1. Therefore, the within-site dispersion of AMS directions in our study is primarily due to natural variation of the magnetic fabric and not instrumental noise. Relatively high susceptibility values indicate that titanomagnetite is the main source of the AMS signal. The magnetic fabric of the Eureka Valley Tuff is generally oblate, with a mean lineation of 1.005 ± 0.004 and a mean foliation of 1.020 ± 0.016 (Fig. 13; Table 6). Ash-flow tuffs commonly exhibit this type of magnetic fabric, where the axis near-normal to the plane of foliation (K_{min}) is presumed to be due to gravity compaction and flow-induced imbrication. The subhorizontal lineation (K_{max}) indicates stretching along the flow path (Ellwood, 1982). In contrast, the AMS results from the lava flows of the Table Mountain Latite and Dardanelles Formation were not useful in determining flow directions. These formations displayed inverted magnetic fabrics with

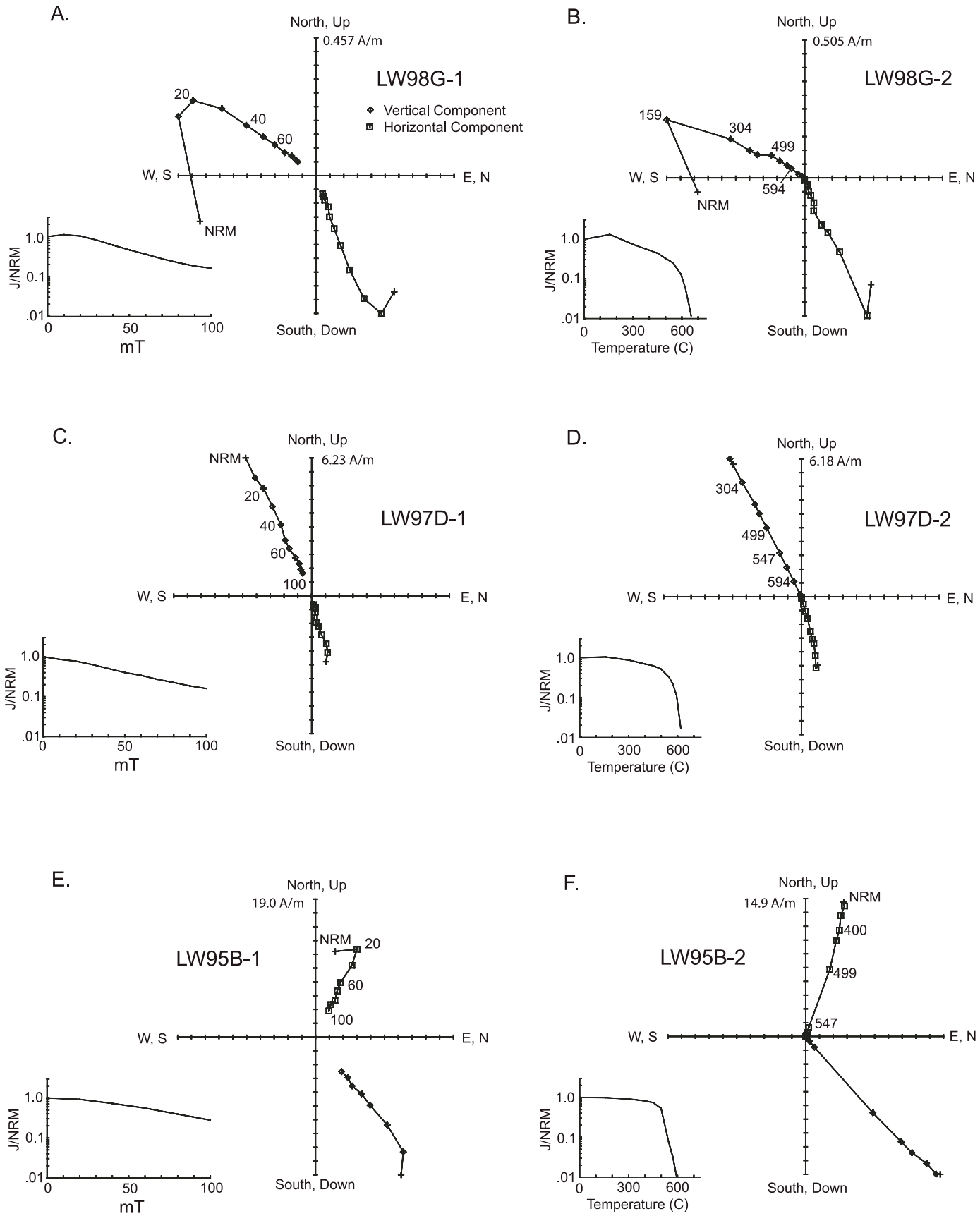

Figure 8. Orthogonal vector diagrams of alternating-field demagnetization (left column) and thermal demagnetization (right column) of selected specimens. Examples are from the Table Mountain Latite (A, B), Tollhouse Flat member of the Eureka Valley Tuff (C, D), and By-Day Member (E, F). J/NRM is ratio of remanent magnetization to initial magnetization.

TABLE 3. REMANENT MAGNETIZATION OF THE STANISLAUS GROUP, CALIFORNIA AND NEVADA

Site				Foliation			Magnetization directions					
Unit	Site	Latitude °N	Longitude °W	Strike, degrees	Dip, degrees	N/N_o	I	D	k	α_{95}	I_c	D_c
Dar	BP5	38.37	119.78	0	0	6/6	67.3	351.2	99.6	6.8		
Dar	WD4	38.36	120.01	0	0	9/9	62.6	338.1	113.5	4.9		
Dar	WD7	38.36	120.01	0	0	6/6	54.2	346.6	69.4	9.3		
Dar	BP7	38.37	119.78	0	0	4/4	57.8	356.7	594.4	3.8		
Tevu	3V156	38.13	119.18	125	22	9/9	9.9	0.0	239.5	3.3	27.5	355.4
Tevu	LW96	38.418	119.368	149	23.7	8/8	14.4	8.4	285.4	3.3	28.3	0.7
Tevb	LW93	38.272	119.288	66.7	23	10/10	33.4	359.1	99.1	4.9	54.0	9.4
Tevb	LW23	38.383	119.438	43.5	8	8/8	44.3	9.3	43.1	8.5	48.4	16.5
Tevb	LW92	38.395	119.528	198.7	24.7	6/6	48.7	31.3	137.9	5.7	48.0	2.9
Tevb	LW95	38.404	119.401	125	17	8/8	43.3	14.1	273.6	3.4	58.7	5.0
Tevt	BP3	38.37	119.78	0	0	6/6	–62.9	154.2	470.5	3.1		
Tevt	LW25	38.398	119.422	56.5	19.5	9/9	–45.0	148.4	48.2	7.5	–64.5	149.6
Tevt	LW90	38.267	119.932	88*	12.3	7/7	–63.5	160.1	193.2	4.4	–74.8	146.5
Tevt	LW91	38.279	119.898	16.3*	17	9/9	–64.3	178.8	138.5	4.4	–64.2	214.9
Tevt	LW94	38.407	119.399	200.3	15	6/6	–63.2	175.9	430.0	3.2	–54.5	155.3
Tevt	LW88	38.206	118.950	11.7	8.7	10/10	–53.9	170.7	52.3	6.7	–56.2	182.8
Tevt	LW86	38.094	119.070	41	9	13/13	–54.4	158.8	91.5	4.4	–62.1	166.5
Tevt	3V138	38.10	119.06	41	9	8/8	–56.2	161.2	470.5	2.6	–63.6	170.6
Tevt	3V129	38.18	118.74	300	8	8/8	–67.0	178.6	197.3	4.0	–59.9	186.1
Tevt	JR	37.93	120.04	0	0	7/7	–42.8	159.1	386.2	3.1		
Tevt	WD10	38.36	120.01	0	0	6/6	–60.0	159.8	352.9	3.6		
Tevt	MK13	38.26	120.30	0	0	9/9	–64.7	158.0	58.1	6.8		
Tevt	LW97	38.14	120.09	0	0	8/8	–62.6	167.3	262.6	3.4		
Ttm	DM11	38.32	119.64	0	0	6/6	–61.6	148.9	378.8	3.5		
Ttm	DM9	38.32	119.64	0	0	6/6	–68.0	134.3	110.3	6.4		
Ttm	DM6	38.32	119.64	0	0	6/6	61.4	6.4	233.0	4.4		
Ttm	DM3	38.32	119.64	0	0	6/6	45.1	357.7	24.7	13.8		
Ttm	DM1	38.32	119.64	0	0	6/6	43.2	356.0	122.3	6.1		
Ttm	MK1	38.25	120.30	0	0	8/8	–20.8	162.1	120.5	5.1		
Ttm	PW26	38.13	120.41	0	0	13/15	–27.0	159.1	144.3	3.5		
Ttm	RH3	38.18	120.36	0	0	6/10	–32.3	177.9	218.0	4.6		
Ttm	WD2	38.35	120.02	0	0	6/6	–26.5	159.3	84.8	7.3		
Ttm	LW98	37.80	120.65	0	0	11/13	–26.7	165.0	300.7	2.6		
Ttm	RR	37.966	120.44	0	0	8	–28.2	164.2	1760	1.3		
Ttm	MC	38.13	120.39	0	0	13	–27.6	162.5	263.1	2.6		
Ttm	LG	38.30	120.125	0	0	11	–26.4	162.7	60.4	6		

Note: Unit labels: Dar—Dardanelles Formation; Tevu—Upper Member of the Eureka Valley Tuff; Tevb—By-Day Member; Tevt—Tollhouse Flat Member; Ttm—Table Mountain Latite. Foliation—attitude of fiamme with downdip direction clockwise from strike value; N/N_o—number of specimens averaged/number of specimens collected; I—inclination in degrees; D—declination in degrees; I_c—inclination corrected for foliation tilt; D_c, declination corrected for foliation tilt; k, estimate of Fisher (1953) precision parameter; α_{95}—radius of 95% confidence circle in degrees.

*Foliation tilt correction not used in final analysis.

K_{min} axes not close to vertical or 95% confidence ellipses of K_{max} greater than 45° (Fig. 12C).

The pre-demagnetized or post-demagnetized results with smaller 95% confidence angles were selected for the flow-direction analysis. We found that pretreatment by AF demagnetization improved the clustering of AMS axes at one lightning-struck site (LW93), where the initial remanence intensity was very strong and the magnetization directions were widely scattered. However, AF pretreatment of the other sites commonly produced little beneficial effect on the AMS scatter and significantly degraded the results at LW96.

DISCUSSION

The study area can be divided into two structural domains—the relatively stable Sierra Nevada block west of Sonora Pass and the tectonically active Walker Lane east of the pass. Although the central Sierra Nevada block is cut by a few north-northwest–striking faults with vertical displacements up to several hundred meters, tilt and vertical-axis rotations beyond the small scale of landslides are negligible. This assertion is supported by the near-concordance of remanent magnetization directions shown by units within the Stanislaus Group over a very broad area. In contrast, the geologic structure is very complex in the Sweetwater Mountains and eastward, and we expect the possibility of vertical axis rotations there. Rotations must be taken into account before interpreting flow directions in the eastern part of the study area, which lies within the Excelsior-Coaldale block of the Walker Lane belt (Stewart, 1988).

The Tollhouse Flat Member is the most widespread member of the Eureka Valley Tuff, and thus provides the best opportunity to test for vertical-axis rotations in the Walker Lane belt. Five sites (MK13, BP3, WD10, LW90, and LW97) in the relatively stable Sierra Nevada

TABLE 4. VIRTUAL GEOMAGNETIC POLES (VGP) FROM THE STANISLAUS GROUP, CALIFORNIA AND NEVADA

Unit	Site	VGP latitude (°N)	VGP longitude (°E)	K	A_{95}	VGP_c latitude (°N)	VGP_c longitude (°E)	VGP_c K	VGP_c A_{95}
Dar	BP5	76.8	214.9	42.6	10.4				
Dar	WD4	72.6	175.5	57.7	6.8				
Dar	WD7	78.7	135.2	47.1	11.3				
Dar	BP7	87.4	151.9	358.0	4.9				
Tevu	3V156	56.9	60.9	575.1	2.4	66.1	71.9	438.7	2.8
Tevu	LW96	58.0	44.9	431.3	2.7	66.7	59.0	364.7	2.9
Tevb	LW93	70.0	63.2	115.6	4.5	81.5	354.3	67.7	5.9
Tevb	LW23	75.3	25.5	39.3	9.0	73.6	359.1	35.1	9.5
Tevb	LW92	62.7	339.8	111.1	6.4	80.3	45.3	113.4	6.3
Tevb	LW95	72.2	14.4	255.7	3.5	86.0	314.3	159.5	4.4
Tevt	BP3	–69.8	355.5	236.5	4.4				
Tevt	LW25	–61.0	315.9	43.1	7.9	–66.4	359.9	22.9	11.0
Tevt	LW90	–73.7	1.1	94.9	6.2				
Tevt	LW91	–82.1	54.1	66.0	6.4				
Tevt	LW94	–83.0	36.0	213.6	4.6	–70.0	328.5	289.1	4.0
Tevt	LW88	–81.7	307.3	35.8	8.2	–87.3	183.2	33.2	8.5
Tevt	LW86	–72.8	327.0	61.6	5.3	–78.5	2.6	47.3	6.1
Tevt	3V138	–75.0	331.6	332.1	3.5	–79.7	18.1	243.0	3.2
Tevt	3V129	–78.4	56.6	88.4	6.7	–84.7	120.3	119.2	4.5
Tevt	JR	–67.9	299.6	365.8	3.2				
Tevt	WD10	–74.3	345.7	196.2	4.8				
Tevt	MK13	–71.8	4.1	27.3	10.0				
Tevt	LW97	–78.9	5.1	133.3	4.8				
Ttm	DM11	–66.1	351.1	199.0	4.8				
Ttm	DM9	–55.7	7.4	45.9	10.0				
Ttm	DM6	83.5	287.5	123.3	6.1				
Ttm	DM3	78.1	70.6	22.0	14.6				
Ttm	DM1	76.4	76.0	114.5	6.3				
Ttm	MK1	–58.2	274.6	171.1	4.3				
Ttm	LW98	–62.8	272.8	394.0	2.3				
Ttm	PW26	–59.8	283.1	188.3	3.0				
Ttm	RH3	–69.3	245.3	260.1	4.2				
Ttm	WD2	–59.6	282.4	111.4	6.4				
Ttm	RR	–63.1	275.1	2253.7	1.3				
Ttm	MC	–61.9	277.7	340.1	2.4				
Ttm	LG	–61.2	276.7	79.5	5.6				

Note: Unit labels: Dar—Dardanelles Formation; Tevu—Upper Member of Eureka Valley Tuff; Tevb—By–Day Member; Tevt—Tollhouse Flat Member; Ttm—Table Mountain Latite. VGP—Virtual geomagnetic pole not corrected for bedding tilt; VGP_c—Virtual geomagnetic pole corrected for bedding tilt; K—Fisher (1953) precision parameter; A_{95}—95% confidence limit, in degrees.

block establish a mean reference direction of magnetization for the Tollhouse Flat Member. We excluded site JR, because it is from a poorly exposed outcrop and may be in a landslide. Late-stage uplift of the Sierra Nevada may have tilted the mountain range less than one degree down to the west (Lindgren, 1911; Huber, 1981; Unruh, 1991; Wakabayashi and Sawyer, 2001), but the amount of tilt is negligible in the context of our study. Positive results from the McFadden and Lowes (1981) similarity test indicate that directions of magnetization from the five sites are indistinguishable at 95% confidence, lending support for this choice of a reference direction. Virtual geomagnetic poles (VGPs) were calculated from each of these sites and averaged together, producing a Sierra Nevada reference pole for the Tollhouse Flat Member (Fig. 14). Likewise, VGPs were calculated for the remaining Tollhouse Flat Member sites and were compared to the Sierra reference VGP for determining vertical-axis rotations and confidence limits following the method of Debiche and Watson (1995).

Results from two sites in the Sweetwater Mountains (LW25 and LW94) indicate no significant vertical-axis rotation of the Tollhouse Flat Member relative to the Sierra reference pole. We can infer that sites in the directly overlying By-Day Member (LW23 and LW95) and Upper Member (LW96) in the Sweetwater Mountains also have not undergone significant vertical-axis rotation. Site 3V156 in the Upper Member at Conway Summit shows no rotation relative to the Sierra block, as inferred from its similarity to the magnetization direction of LW96. In contrast, sites near Mono Lake, Bodie, and Anchorite Hills (Fig. 7) indicate significant clockwise rotations at the 95% confidence level. Sites in the Tollhouse Flat Member (LW88, 3V138, and 3V129) have rotated clockwise 23° ± 9°, 10° ± 5°, and 26° ± 6°, respectively. These rotations are taken into account in our interpretation of the AMS results and the regional patterns of flow within the Eureka Valley Tuff (Figs. 15 and 16).

Clockwise rotation of the Bodie-Anchorite Hills area agrees with predictions made by Wesnousky (2005), who analyzed Quaternary faulting within the east-trending Excelsior-Coaldale block (Fig. 16) of the central Walker Lane. He proposed that left-lateral faults, such as the Anchorite Pass fault, represented Reidel shears cutting across a right step within the dextral shear zone of the Walker Lane. According to the model, the left-lateral faults formed as conjugates aligned 30° off the maximum axis of compression, and the faults rotated 20°–30° clockwise to accommodate dextral shear in the Walker Lane. Cashman and Fontaine (2000) reported paleomagnetic evidence of clockwise rotation of Miocene volcanic rocks in the Carson block, which is structurally similar to the Excelsior-Coaldale block, but is located farther north within the Walker Lane. Our paleomagnetic results lend

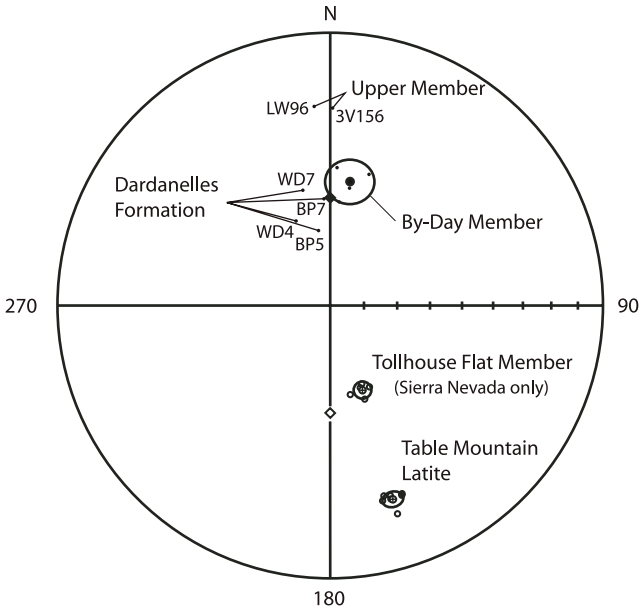

Figure 9. Site-mean directions (small circles and dots) and formation means (larger dot and crossed circles) with 95% confidence limits from the Stanislaus Group. Sites DM 1–11 and RH3 are excluded from diagram and are not used in calculation of Table Mountain Latite mean. Equal-area projection—dots are normal polarity sites plotted on lower hemisphere; circles are reversed-polarity sites plotted on upper hemisphere. Solid and open diamonds represent normal- and reversed-axial dipole fields, respectively.

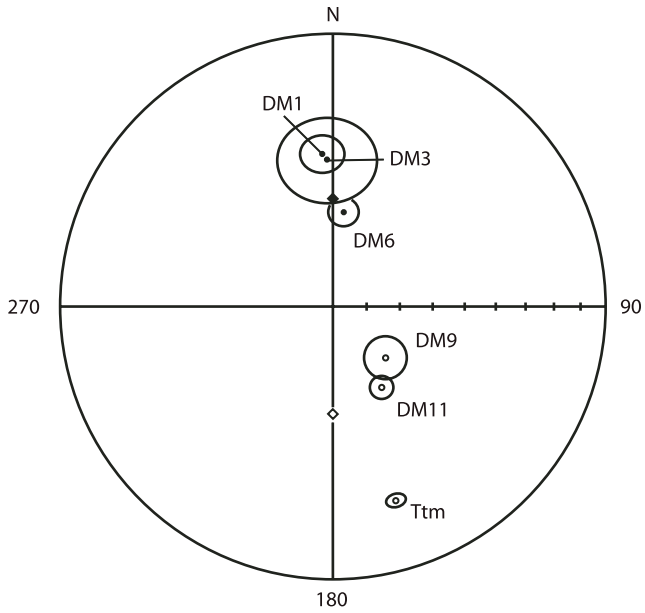

Figure 10. Site-mean directions of magnetization and 95% confidence limits for sites DM 1–11 in the Table Mountain Latite near Leavitt Peak, California. Ttm—mean direction from the Table Mountain Latite on the western slope of the Sierra Nevada. Dots are on the lower hemisphere; circles are on the upper hemisphere. Solid and open diamonds represent normal- and reversed-axial dipole fields, respectively.

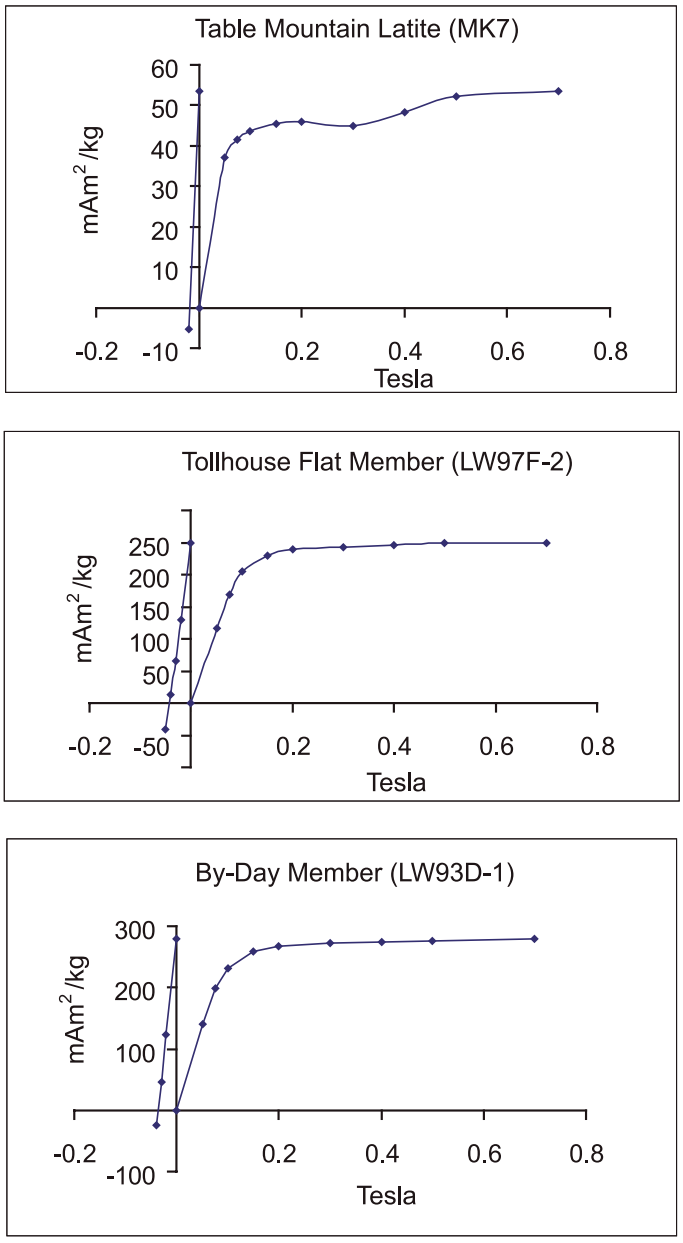

Figure 11. Acquisition of isothermal remanent magnetization (IRM) for three specimens from the Table Mountain Latite and Eureka Valley Tuff.

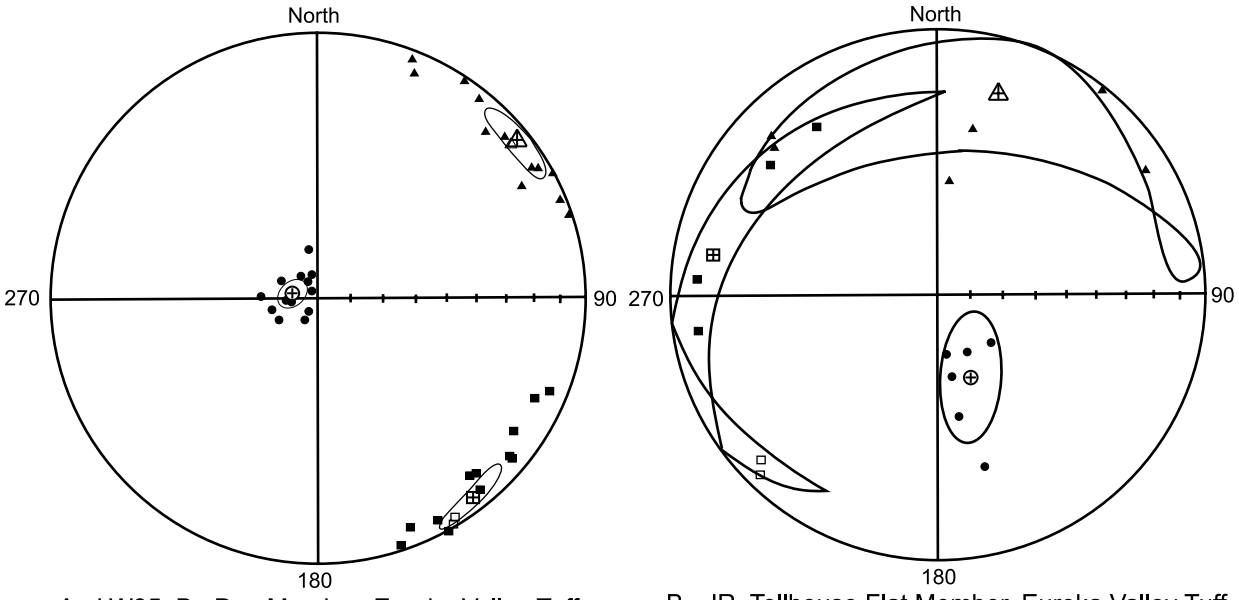

A. LW95, By-Day Member, Eureka Valley Tuff

Axis	I	D	a(95)minor	a(95)major
⊞ Mean Kmax	5.9	142.3	3.2	10.5
⧋ Mean Kint	5.1	51.8	4.8	10.4
⊕ Mean Kmin	82.2	281.3	3.7	5.1

B. JR, Tollhouse Flat Member, Eureka Valley Tuff

Axis	I	D	a(95)minor	a(95)major
⊞ Mean Kmax	15.5	280.2	8.2	76.8
⧋ Mean Kint	22.0	16.6	19.6	76.8
⊕ Mean Kmin	62.6	157.9	8.7	20.7

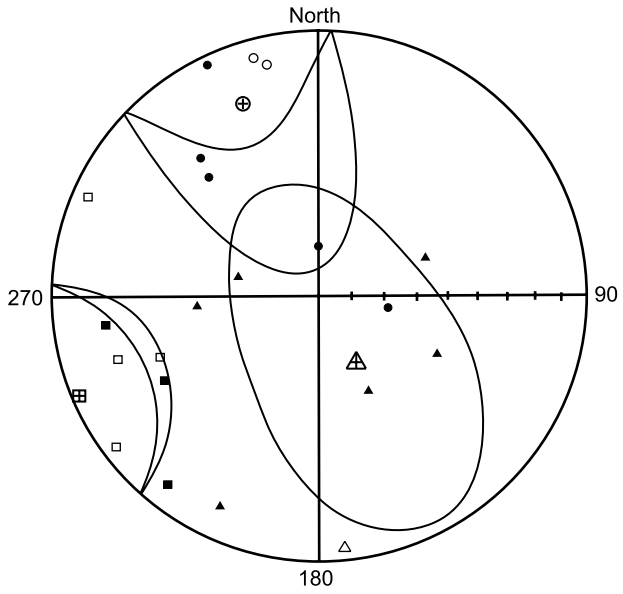

C. WD7, Dardanelles Formation

Axis	I	D	a(95)minor	a(95)major
⊞ Mean Kmax	2.8	247.3	25.0	33.7
⧋ Mean Kint	66.4	150.8	31.6	61.4
⊕ Mean Kmin	23.4	338.5	27.1	61.3

Figure 12. Examples of anisotropy of magnetic susceptibility (AMS) data from three sites in the Stanislaus Group. Smaller symbols indicate specimen data; crossed symbols denote principal axis means with 95% confidence ellipses. Equal area projections with solid symbols in lower hemisphere; open symbols in upper hemisphere.

TABLE 5. PRINCIPAL COMPONENTS OF ANISOTROPY OF MAGNETIC SUSCEPTIBILITY (AMS) FROM THE EUREKA VALLEY TUFF, CALIFORNIA AND NEVADA

Site	N_o	N	AF	K_{max}				K_{int}				K_{min}			
				I	D	$\alpha_{(95)}$ min	$\alpha_{(95)}$ max	I	D	$\alpha_{(95)}$ min	$\alpha_{(95)}$ max	I	D	$\alpha_{(95)}$ min	$\alpha_{(95)}$ max
LW96	10	10	No	7.7	136.5	3.9	10.8	19.7	229.3	8.8	10.9	68.8	26.2	3.6	9.0
3V156	9	7	Yes	5.8	347.6	2.7	24.0	3.7	257.2	6.7	24.5	83.1	134.9	3.1	8.6
LW92	6	6	Yes	9.0	215.4	5.0	63.1	11.8	123.5	32.3	63.1	75.1	341.6	4.6	32.4
LW93	5	4	Yes	9.6	11.5	11.9	38.7	4.1	280.8	13.9	16.8	79.5	168.1	7.7	39.8
LW23	8	5	No	17.9	208.8	15.0	22.9	3.5	117.7	20.8	28.4	71.8	17.1	11.7	28.7
LW95	15	14	No	5.9	142.3	3.2	10.5	5.1	51.8	4.8	10.4	82.2	281.3	3.7	5.1
LW90	7	5	No	9.9	88.7	5.8	20.3	7.1	357.4	12.2	20.2	77.8	232.3	3.2	13.3
LW94	10	9	Yes	14.7	149.1	3.5	38.7	10.9	56.2	7.2	38.9	71.5	290.9	4.6	10.2
WD10	6	5	Yes	10.0	72.1	2.1	8.3	1.5	162.3	7.0	13.9	79.9	260.6	2.4	13.3
3V129	14	10	No	0.9	170.0	7.9	24.4	3.4	260.1	6.8	24.3	86.5	65.6	3.2	10.2
3V138	9	9	No	9.1	290.2	9.4	44.7	4.5	20.9	7.6	44.4	79.8	137.2	6.7	13.0
BP3	6	6	Yes	7.5	22.4	15.9	73.9	0.8	292.3	12.8	73.9	82.5	196.3	12.9	16.2
JR	7	6	Yes	15.5	280.2	8.2	76.8	22.0	16.7	19.6	76.8	62.6	157.9	8.7	20.7
LW91	9	8	No	10.0	93.2	10.1	22.8	0.3	3.2	6.9	23.2	80.0	271.7	7.0	12.3
LW88	10	8	Yes	5.1	259.1	5.4	15.8	0.3	169.1	4.3	16.1	84.9	76.3	3.7	6.7
LW25	9	8	No	5.3	73.7	9.8	40.7	1.5	343.5	5.4	40.7	84.5	237.9	5.2	10.1
MK13	14	12	No	1.1	33.3	6.9	17.8	8.1	303.2	4.4	18.2	81.8	130.6	6.8	8.0
LW86	13	11	No	8.3	353.3	5.5	22.9	5.1	262.6	5.8	22.8	80.3	141.6	3.2	8.3
LW97	13	13	No	10.3	75.0	4.0	12.5	13.4	167.5	5.0	13.1	73.0	308.7	3.8	6.5

Note: N_o— number of specimens measured; N—number of specimens averaged; AF—alternating-field pre-treatment; I—inclination; and D—declination of principal AMS axes in degrees, after tilt correction. The $\alpha_{(95)}$min and $\alpha_{(95)}$max are the lengths of the minor and major axes, respectively, of the 95% confidence ellipses in degrees.

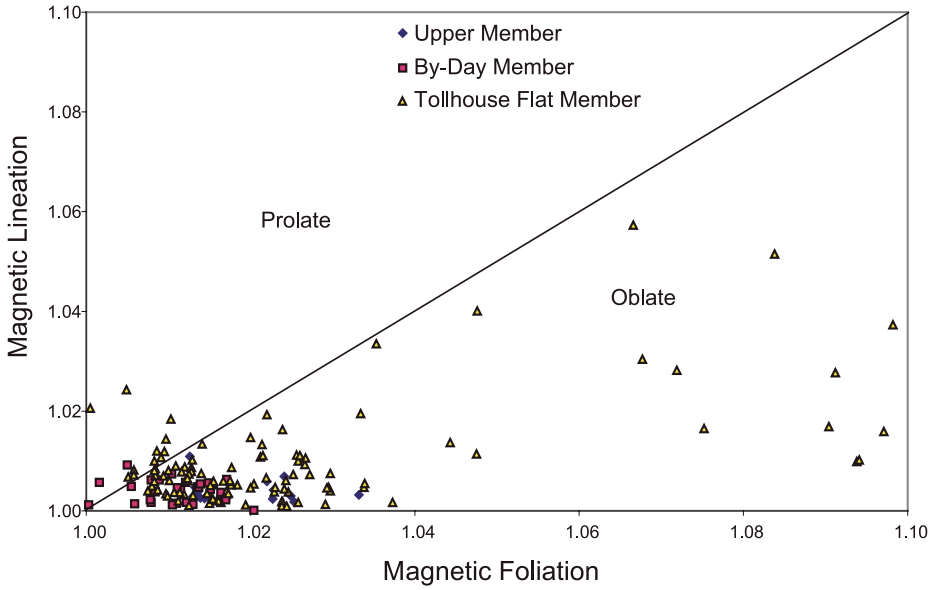

Figure 13. Magnetic foliation versus magnetic lineation of specimens from the Eureka Valley Tuff.

support to Wesnousky's (2005) interpretation, although the supporting evidence comes from only three sites. A substantial part of Eureka Valley Tuff east of Bridgeport Reservoir remains to be sampled for paleomagnetism, offering an opportunity to attempt a more rigorous test of the kinematic model.

How do rotation rates derived from paleomagnetic data in this region compare with modern rotations due to the interaction between the Pacific and North America plates? Contemporary GPS velocity measurements show the Sierra Nevada block to be moving northwest (313°) approximately 12 mm/year relative to the Colorado Plateau and the stable North America plate (Bennett et al., 2003). Large-scale spherical caps, such as the Sierra Nevada and the western Great Basin, are rotating clockwise relative to stable North America at rates on the order of 0.3°/million years (McCaffrey, 2005), and the rate of differential rotation between the Sierra Nevada and western Great Basin blocks is even less. The current Sierra Nevada rotation rate is much greater than its long-term average, as indicated by the relatively small clockwise rotation (6° ± 8° relative to stable North America) determined from Frei's (1986) paleomagnetic study of Cretaceous granites in the Sierra Nevada. In contrast, paleomagnetism of our sites in the eastern part of the Eureka Valley Tuff indicates that the average rotation rate is ~2.5°/m.y. since 9.5 Ma. The relatively high rotation rate found

TABLE 6. MEAN ANISOTROPY OF MAGNETIC SUSCEPTIBILITY (AMS) PARAMETERS FROM THE EUREKA VALLEY TUFF, CALIFORNIA AND NEVADA

Site	Magnetic susceptibility (SI), lineation, and foliation						Jelinek (1978) parameters	
	K_{max}	K_{int}	K_{min}	K_{mean}	L	F	P_J	T
LW96	0.016006	0.015965	0.015716	0.0159	1.0026	1.0159	1.016	0.720
3V156	0.019828	0.019752	0.019315	0.0196	1.0039	1.0226	1.023	0.705
LW92	0.017920	0.017884	0.017729	0.0178	1.0020	1.0087	1.009	0.621
LW93	0.036142	0.036070	0.035892	0.0360	1.0015	1.0050	1.005	0.532
LW23	0.014271	0.014159	0.014081	0.0142	1.0079	1.0055	1.012	-0.181
LW95	0.023317	0.023224	0.022907	0.0231	1.0040	1.0139	1.015	0.552
LW90	0.022166	0.022013	0.021558	0.0219	1.0069	1.0211	1.024	0.502
LW94	0.017502	0.017414	0.017111	0.0173	1.0050	1.0177	1.019	0.555
WD10	0.029318	0.029119	0.028357	0.0289	1.0069	1.0269	1.029	0.590
3V129	0.026425	0.026212	0.025452	0.0260	1.0081	1.0299	1.032	0.569
3V138	0.020211	0.020130	0.019891	0.0201	1.0040	1.0120	1.014	0.497
BP3	0.024114	0.024099	0.023777	0.0240	1.0006	1.0135	1.012	0.910
JR	0.008726	0.008692	0.008436	0.0086	1.0040	1.0302	1.029	0.766
LW91	0.025293	0.025177	0.024846	0.0251	1.0046	1.0133	1.015	0.482
LW88	0.025382	0.025300	0.024706	0.0251	1.0032	1.0241	1.023	0.761
LW25	0.023387	0.023291	0.022871	0.0232	1.0041	1.0183	1.019	0.632
MK13	0.010515	0.010286	0.009539	0.0101	1.0223	1.0784	1.086	0.548
LW86	0.018333	0.018193	0.017987	0.0182	1.0077	1.0115	1.016	0.198
LW97	0.027259	0.027146	0.026871	0.0271	1.0042	1.0102	1.012	0.420

Note: $K_{mean} = (K_{max} + K_{int} + K_{min})/3$; L—magnetic lineation; F—magnetic foliation; P_J—degree of anisotropy; T—shape parameter.

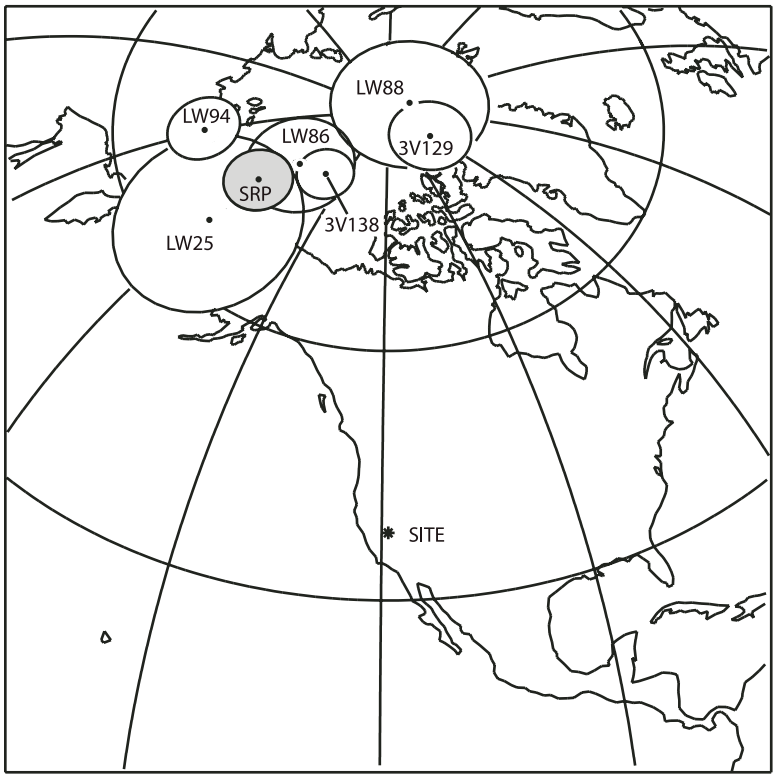

Figure 14. Virtual geomagnetic poles (VGP) from eastern sites within the Tollhouse Flat Member (Eureka Valley Tuff) are compared with the Sierra Nevada reference VGP (SRP) to detect vertical-axis rotations. Given the 95% confidence limits (ellipses), sites 3V138, 3V129, and LW88 are rotated clockwise significantly.

in our study is likely an indication of localized dextral shear operating on small-scale blocks caught within the western Walker Lane-Sierra Nevada transition, and the rotation may have occurred during a brief but intense interval of activity. However, current coverage by GPS monitors is too sparse to define the boundaries and modern rotation rates of small blocks in the Mono Lake region for comparison with paleomagnetic data.

As indicated by the AMS results, flow directions are generally outward from the Little Walker Caldera and are consistent with the alignments and slopes of several known channels or paleovalleys (Fig. 15). The imbrication of the K_{max}–K_{int} plane indicates the sense of flow, analogous to streambed imbrication where the upper surfaces of flat cobbles dip upstream. The pyroclastic flows of the Tollhouse Flat Member flowed down at least two paleovalleys to the west and to the southeast toward Mono Basin and Anchorite Hills. Ransome (1898) described the Cataract Channel, which he traced upstream from Knights Ferry in the Sierran foothills to Dardanelles Cone, and Slemmons (1953) extended the course of the channel eastward to Sonora Peak. The AMS flow indicators from the Tollhouse Flat Member at sites MK13 and WD10 are consistent with westward flow down the Cataract Channel. At site BP3, the imbrication and azimuth are very poorly constrained and do not follow the channel morphology. Tollhouse Flat Member sites LW90, LW91,

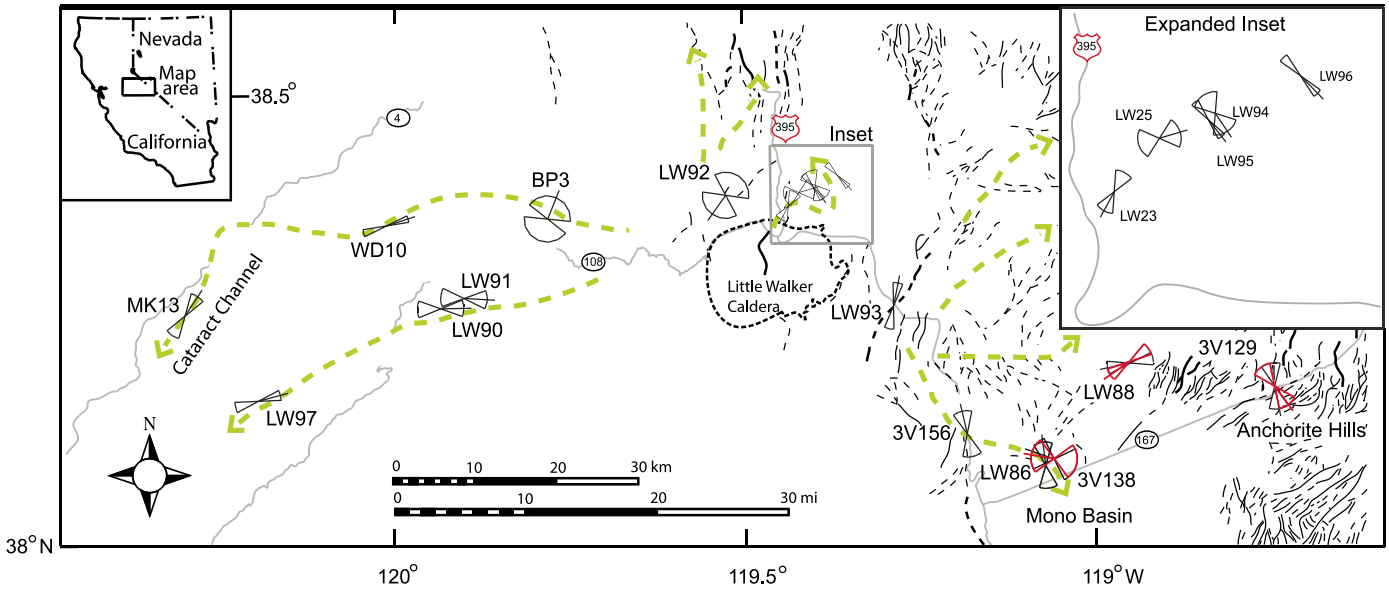

Figure 15. AMS flow indicators are depicted as fans aligned with the maximum principal axis of magnetic susceptibility; width of the fan shows the 95% confidence limit of the azimuth. Tick mark on fan, based on imbrication of magnetic foliation plane, points upstream. Red symbols show AMS indicator corrected for vertical-axis rotation. Dashed green lines indicate channel forms in Eureka Valley Tuff, as inferred from outcrop patterns (Fig. 1) and Slemmons (1966; his Fig. 3). Fine-line faults are modified from Dohrenwend (1982). Heavy-line faults are adapted from Stewart (1978).

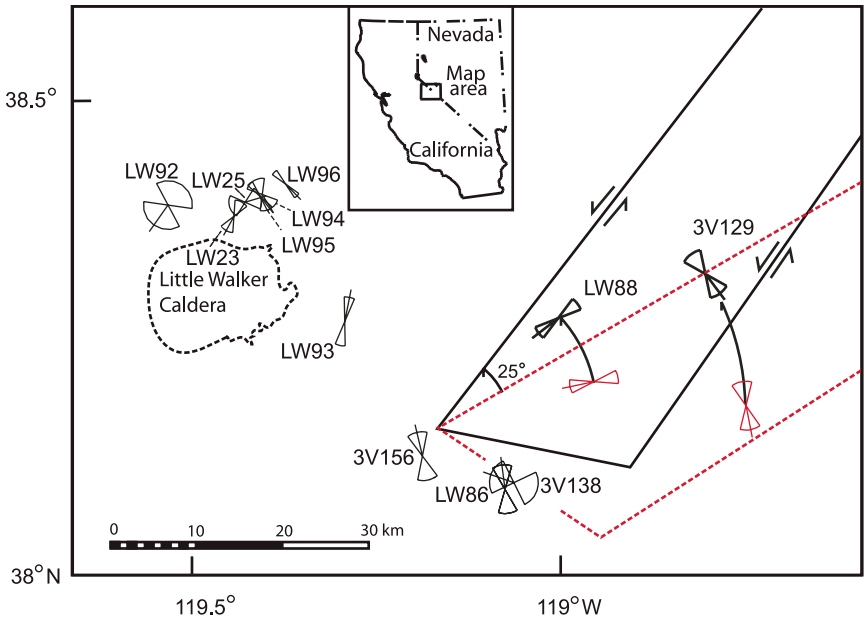

Figure 16. Tectonic model of the eastern study area showing original positions (heavy black symbols) and AMS data of LW88 and 3V129 after removing 25° of vertical-axis rotation of the southwestern part of the Excelsior-Coaldale block (Stewart, 1988). Model assumes left-lateral faults were rotated clockwise during dextral shear of the Walker Lane as proposed by Wesnousky (2005).

and LW97 indicate westward flow down an unnamed paleovalley that is south of the Cataract Channel.

The Sweetwater Mountains appear to have been a topographic high during the eruptions of the Table Mountain Latite lavas and the pyroclastic flows of the Eureka Valley Tuff, preventing these eruptions from flowing much farther than a few miles northeast of the Little Walker Caldera. This pattern was discussed by Halsey (1953), who also observed that outcrops of these formations lap up against the western and southeastern flanks of the Sweetwater Mountains. Sites LW94, LW95, and LW96, which represent three distinct ash-flow eruptions, indicate northwest flow parallel to the range front of the Sweetwater Mountains. Site LW23's northeasterly direction of flow radiates outward from the Little Walker Caldera, but is nearly opposite to the flow indicator at LW25. This contradiction may be attributed to run-up of the pyroclastic flow onto the margin of a paleochannel or large uncertainty in the imbrication orientation at LW25.

Sites LW93 and 3V156 indicate a direction of flow to the south during the eruptions of the By-Day and Upper Members of the Eureka Valley Tuff. In the Bodie Hills, sites LW88 and LW86 (in the Tollhouse Flat Member) indicate

directions of flow to the east and south, respectively. The far eastern site near the Anchorite Hills, 3V129, has a flow direction to the north. Southward flow inferred at LW86, LW93, and 3V156 is generally compatible with a channel leading south from the Little Walker Caldera. Interpretation of the flow pattern at the eastern sample sites is complicated by probable northward displacement of the caldera relative to the eastern sites due to dextral shear across the area. In the northern Walker Lane, offsets of Oligocene paleovalleys indicate cumulative slip of 20–30 km since 9 Ma (Faulds et al., 2005). We do not have comparable measurements of dextral displacement across our study area east of the Little Walker Caldera, because the fault pattern in general is not parallel to the dominant northwest-striking, right-lateral faults of the Walker Lane. Instead, the shear strain is being accommodated by compression and clockwise rotation across the Excelsior-Coaldale domain. The Little Walker Caldera is probably moving with the Sierra block, although bounding faults are not well defined in this part of the Sierra-Walker Lane transition. Restoring the original positions of sites LW88 and 3V129 relative to the caldera by removing 25° of rotation brings the sites closer to an east-west alignment with the caldera (Fig. 16). Eastward flow from the caldera could explain the flow indicator at LW88, but the northwest flow restored at 3V129 is transverse to this pattern.

Palmer and MacDonald (1999) propose a model to explain variation in K_{max} declinations (flow directions) with distance from the source caldera. In this model, there is a proximal zone of converging flow (tributaries), an intermediate channelized zone, and a distal zone of diverging flow (distributaries). This model implies larger scatter in the K_{max} declinations in proximal and distal zones as compared to the intermediate channelized zones. This variation model is a possible explanation for the conflicting flow directions at sites near the Little Walker Caldera (LW23, LW25, LW94, LW95, and LW96). However, weak development of flow fabric and failure of AMS to always be an accurate flow indicator are also possible, as noted by MacDonald and Palmer (1990), Wells and Hillhouse and Wells (1991), and Le Pennec et al. (1998). Ort (1993) reported that a small percentage of K_{max} axes were transverse to the dominant flow axis in an Andean ash-flow tuff.

CONCLUSION

The AMS results generally follow a pattern of pyroclastic flow outward from the Little Walker Caldera, as proposed by Noble et al. (1974) and by Priest (1979). AMS lineations and imbrications in the Eureka Valley Tuff are generally consistent with the mapped trends of Miocene channels in the Stanislaus River drainage. The pyroclastic flows followed preexisting topography to the west and southwest, and to the east and southeast. The AMS results appear to be more dispersed near the source area and at the eastern distal ends of the pyroclastic flows in comparison with the channelized flows. The pyroclastic flows of the Eureka Valley Tuff followed a network of canyons, including the Cataract Channel, leading to long runout distances from the eruptive center (~60 km to the west).

The model that the central Sierra Nevada is a rigid block (Huber, 1990; Wakabayashi and Sawyer, 2001) is supported by the paleomagnetic data. Remanent magnetization directions of the Tollhouse Flat Member collected at five locations from the western foothills to the Sierra Nevada crest have the same direction at the 95% confidence level. The Tollhouse Flat reference VGP produced as part of this study was used to describe rotations within the Walker Lane at sampling sites in the Bodie Hills, Mono Basin, and Anchorite Hills. These rotations are ~10° to 26° clockwise with respect to the Sierra Nevada block, which is in agreement with recent estimates of rotation within the central Walker Lane (Wesnousky, 2005). East-trending, left-lateral faults within the Excelsior-Coaldale block of the Walker Lane were rotated into present alignments as a probable consequence of dextral shear across the Sierra Nevada-Walker Lane transition. Further paleomagnetic study of Stanislaus Group outcrops near the California-Nevada border should help to define the extent of the highly rotated region and provide the basic framework for neotectonic studies.

The different remanent magnetization directions within the Stanislaus Group can be used to distinguish among these volcanic formations. In the western Sierra Nevada, the Table Mountain Latite has a magnetization direction of I = –26.1°, D = 163.1° (α_{95} = 2.7°), which is unusual with respect to the axial dipole. As originally shown by Al-Rawi (1969), the Tollhouse Flat Member of the Eureka Valley Tuff has a reversed-polarity magnetization direction in contrast to the normal polarity directions of the By-Day Member and the Upper Member. The Dardanelles Formation has a normal-polarity magnetization direction, which helps to distinguish this formation from the similar Table Mountain Latite. Further work is needed to determine whether the magnetostratigraphy of the Table Mountain Latite and the Dardanelles Formation is actually more complex, as suggested by samples collected at Sonora Pass (DM1–DM11).

ACKNOWLEDGMENTS

This research was part of the principal author's M.S. thesis (B.P. Hausback, faculty advisor) with partial financial support from EDMAP (the Educational Component of the National Cooperative Geologic Mapping Program). Gromme was assisted in the field in 1962 by Robert J. Fleck and Ronald T. Merrill. That work and the preliminary measurements were unstintingly supported by the late Professor John Verhoogen, University of California, under National Science Foundation Grant GF74, which is gratefully acknowledged. Edward A. Mankinen (USGS) was very helpful in locating original data and providing site locations of the Cox collection. We thank Joe Rosenbaum (USGS), David John (USGS), Ray Wells (USGS), Bernie Housen (Western Washington University), and an anonymous reviewer for thoughtful suggestions to improve the manuscript. We acknowledge Myrl Beck for sharing unpublished data from the first (1960) paleomagnetic study of the Table Mountain Latite.

REFERENCES CITED

Al-Rawi, Y.T., 1969, Cenozoic history of the northern part of Mono Basin, California and Nevada [Ph.D. thesis]: Berkeley, California, University of California, 163 p.

Argus, D.F., and Gordon, R.G., 1991, Current Sierra Nevada-North America motion from very long baseline interferometry: Implications for the kinematics of the western United States: Geology, v. 19, p. 1085–1088, doi: 10.1130/0091-7613(1991)019<1085:CSNNAM>2.3.CO;2.

Atwater, T., and Stock, J., 1998, Pacific-North America plate tectonics of the Neogene southwestern United States: An update: International Geology Review, v. 40, p. 375–402.

Baer, E.M., Fisher, R.V., Fuller, M., and Valentine, G., 1997, Turbulent transport and deposition of the Ito pyroclastic flow: Determinations using anisotropy of magnetic susceptibility: Journal of Geophysical Research, v. 102, p. 22,565–22,586, doi: 10.1029/96JB01277.

Bennett, R.A., Wernicke, B.P., Niemi, N.A., and Friedrich, A.M., 2003, Contemporary strain rates in the northern Basin and Range province from GPS data: Tectonics, v. 22, no. 2, p. 1008, doi: 10.1029/2001TC001355.

Brem, G.F., 1977, Petrogenesis of late Tertiary potassic volcanic rocks in the Sierra Nevada and western Great Basin [Ph.D. thesis]: Riverside, University of California, 361 p.

Brem, G.F., 1984, Geologic map of the Sweetwater Roadless area, California and Nevada: U.S. Geological Survey Miscellaneous Field Studies Map MF-1535-B, scale 1:62,500, 1 sheet.

Cashman, P.H., and Fontaine, S.A., 2000, Strain partitioning in the northern Walker Lane, western Nevada and northeastern California: Tectonophysics, v. 326, p. 111–130, doi: 10.1016/S0040-1951(00)00149-9.

Chesterman, C.W., 1968, Volcanic geology of the Bodie Hills, Mono County, California, *in* Coats, R.R., Hay, R.C., and Anderson, C.A., eds., Studies in volcanology: Geological Society of America Memoir 166, p. 45–68.

Cogné, J.P., 2003, PaleoMac: A Macintosh application for treating paleomagnetic data and making plate reconstructions: Geochemistry, Geophysics, Geosystems, v. 4, no. 1, doi: 10.1029/2001GC000227.

Dalrymple, G.B., 1963, Potassium-argon dates of some Cenozoic volcanic rocks of the Sierra Nevada, California: Geological Society of America Bulletin, v. 74, p. 379–390, doi: 10.1130/0016-7606(1963)74[379:PDOSCV]2.0.CO;2.

Dalrymple, G.B., 1964, Cenozoic chronology of the Sierra Nevada: University of California Publications in Geological Sciences, v. 47, 39 p.

Dalrymple, G.B., Cox, A., Doell, R.R., and Gromme, C.S., 1967, Pliocene geomagnetic polarity epochs: Earth and Planetary Science Letters, v. 2, p. 163–173, doi: 10.1016/0012-821X(67)90122-7.

Debiche, M.G., and Watson, G.S., 1995, Confidence limits and bias correction for estimating angles between directions with applications to paleomagnetism: Journal of Geophysical Research, v. 100, B12, p. 24,405–24,429, doi: 10.1029/92JB01318.

Dohrenwend, J.C., 1982, Map showing late Cenozoic faults in the Walker Lake 1º by 2º quadrangle, Nevada-California: U.S. Geological Survey Miscellaneous Field Studies Map MF-1382-D, scale 1:250,000, 1 sheet.

Ellwood, B.B., 1982, Estimates of flow directions for calc-alkaline welded tuffs and paleomagnetic data reliability from anisotropy of magnetic susceptibility measurements: central San Juan Mountains, southwest Colorado: Earth and Planetary Science Letters, v. 59, p. 303–314, doi: 10.1016/0012-821X(82)90133-9.

Elston, W.E., and Smith, E.I., 1970, Determination of flow direction of rhyolitic ash-flow tuffs from fluidal textures: Geological Society of America Bulletin, v. 81, p. 3393–3406, doi: 10.1130/0016-7606(1970)81[3393:DOFDOR]2.0.CO;2.

Faulds, J.E., Henry, C.D., and Hinz, N.H., 2005, Kinematics of the northern Walker Lane: An incipient transform fault along the Pacific-North American plate boundary: Geology, v. 33, p. 505–508, doi: 10.1130/G21274.1.

Fisher, R.A., 1953, Dispersion on a sphere: Proceedings of the Royal Society of London, Series A, v. 217, p. 295–305.

Frei, L.S., 1986, Additional paleomagnetic results from the Sierra Nevada: Further constraints on Basin and Range extension and northward displacement in the western United States: Geological Society of America Bulletin, v. 97, p. 840–849, doi: 10.1130/0016-7606(1986)97<840:APRFTS>2.0.CO;2.

Gilbert, C.M., Christensen, M.N., Al-Rawi, Y., and Lajoie, K.R., 1968, Structural and volcanic history of Mono Basin, California-Nevada, *in* Coats, R. R., Hay, R.C., and Anderson, C.A., eds., Studies in volcanology: Geological Society America Memoir 116, p. 275–329.

Giusso, J.R., 1981, Preliminary geologic map of the Sonora Pass 15-minute quadrangle, California: U.S. Geological Survey Open-File Report 81-1170, scale 1:24,000, 1 sheet.

Gromme, C.S., McKee, E.H., and Blake, M.C., Jr., 1972, Paleomagnetic correlations and potassium argon dating of middle Tertiary ash-flow sheets in the eastern Great Basin: Geological Society of America Bulletin, v. 83, p. 1619–1638, doi: 10.1130/0016-7606(1972)83[1619:PCAPDO]2.0.CO;2.

Halsey, J.G., 1953, Geology of parts of the Bridgeport, California and Wellington, Nevada quadrangles [Ph.D. thesis]: Berkeley, University of California, 506 p.

Hearn, E.H., and Humphreys, E.D., 1998, Kinematics of the southern Walker Lane Belt and motion of the Sierra Nevada block: Journal of Geophysical Research, v. 103, no. B11, p. 27,033–27,049, doi: 10.1029/98JB01390.

Hext, G., 1963, The estimation of second-order tensors, with related tests and designs: Biometrika, v. 50, p. 353–357.

Hillhouse, J.W., and Wells, R.E., 1991, Magnetic fabric, flow directions, and source area of the lower Miocene Peach Springs Tuff in Arizona, California, and Nevada: Journal of Geophysical Research, v. 96, no. B7, p. 12,443–12,460.

Huber, N.K., 1981, Amount and timing of Late Cenozoic uplift and tilt of the central Sierra Nevada, California-Evidence from the Upper San Joaquin River Basin: U.S. Geological Survey Professional Paper 1197, 28 p.

Huber, N.K., 1983a, Preliminary geologic map of the Dardanelles Cone quadrangle, central Sierra Nevada, California: U.S. Geological Survey Miscellaneous Field Studies Map MF-1436, scale 1:62,500, 1 sheet.

Huber, N.K., 1983b, Preliminary geologic map of the Pinecrest quadrangle, central Sierra Nevada, California: U.S. Geological Survey Miscellaneous Field Studies Map MF-1437, scale 1:62,500, 1 sheet.

Huber, N.K., 1990, The Late Cenozoic evolution of the Tuolumne River, central Sierra Nevada, California: Geological Society of America Bulletin, v. 102, p. 102–115, doi: 10.1130/0016-7606(1990)102<0102:TLCEOT>2.3.CO;2.

Huber, N.K., Bateman, P.C., and Wahrhaftig, C., 1989, Geologic map of Yosemite National Park and vicinity, California: U.S. Geologic Survey Miscellaneous Investigations Series Map I-1874, scale 1:125,000, 1 sheet.

Incoronato, A., Addison, F.T., Tarling, D.H., Nardi, G., and Pescatore, T., 1983, Magnetic fabric investigation of pyroclastic deposits from Phlegrean Fields, southern Italy: Nature, v. 306, p. 461–463, doi: 10.1038/306461a0.

Irvine, T.N., and Baragar, W.R.A., 1971, A guide to the chemical classification of the common volcanic rocks: Canadian Journal of Earth Sciences, v. 8, p. 523–548.

Jelinek, V., 1978, Statistical processing of magnetic susceptibility measured in groups of specimens: Studia Geophysica et Geodetica, v. 22, p. 50–62, doi: 10.1007/BF01613632.

Johnson, R.F., 1951, Geology of the Masonic mining district, Mono County, California [M.A. thesis]: Berkeley, California, University of California, 55 p.

King, N.K., 2006, Stratigraphy, paleomagnetism, geochemistry, and anisotropy of magnetic susceptibility of the Miocene Stanislaus Group, central Sierra Nevada and Sweetwater Mountains, California and Nevada [M.S. thesis]: Sacramento, California, California State University, 81 p.

Kirschvink, J.L., 1980, The least-squares line and plane and the analysis of palaeomagnetic data: Geophysical Journal of the Royal Astronomical Society, v. 62, p. 699–718.

Kleinhampl, F.J., Davis, W.E., Silberman, M.L., Chesterman, C.W., Chapman, R.H., and Gray, C.H., Jr., 1975, Aeromagnetic and limited gravity studies and generalized geology of the Bodie Hills region, Nevada and California: U.S. Geological Survey Bulletin 1384, scale 1:125,000, 1 sheet, 38 p.

Knight, M.D., Walker, G.P.L., Ellwood, B.B., and Diehl, J.F., 1986, Stratigraphy, paleomagnetism, and magnetic fabric of the Toba Tuffs: Constraints on the sources and eruptive styles: Journal of Geophysical Research, v. 91, p. 10,355–10,382.

Le Bas, M.J., Le Maitre, R.W., Streckeisen, A., and Zenettin, B., 1986, A chemical classification of volcanic rocks based on the total alkali-silica diagram: Journal of Petrology, v. 27, p. 745–750.

Le Pennec, J.L., Chen, Y., Diot, H., Froger, J., and Gourgaud, A., 1998, Interpretation of anisotropy of magnetic susceptibility fabric of ignimbrites in terms of kinematic and sedimentological mechanisms: An Anatolian case-study: Earth and Planetary Science Letters, v. 157, p. 105–127, doi: 10.1016/S0012-821X(97)00215-X.

Lienert, B.R., 1991, Monte Carlo simulation of errors in the anisotropy of magnetic susceptibility: A second-rank symmetric tensor: Journal of Geophysical Research, v. 96, p. 19,539–19,544.

Lindgren, W., 1911, The Tertiary gravels of the Sierra Nevada of California: U.S. Geological Survey Professional Paper 73, 226 p.

MacDonald, W.D., and Palmer, H.C., 1990, Flow directions in ash-flow tuffs: A comparison of geological and magnetic susceptibility measurements, Tshirege member (upper Bandelier Tuff), Valles caldera, New Mexico, USA: Bulletin of Volcanology, v. 53, p. 45–59, doi: 10.1007/BF00680319.

McCaffrey, R., 2005, Block kinematics of the Pacific-North America plate boundary in the southwestern United States from inversion of GPS, seismological, and geologic data: Journal of Geophysical Research, v. 110, B07401, doi:10.1029/2004JB003307, 27 p.

McFadden, P.L., and Lowes, F.J., 1981, The discrimination of mean directions drawn from Fisher distributions: Geophysical Journal of the Royal Astronomical Society, v. 67, p. 19–33.

McFadden, P.L., and McElhinny, M.W., 1988, The combined analysis of remagnetization circles and direct observations in palaeomagnetism: Earth and Planetary Science Letters, v. 87, no. 1–2, p. 161–172, doi: 10.1016/0012-821X(88)90072-6.

McQuarrie, N., and Wernicke, B.P., 2005, An animated tectonic reconstruction of southwestern North America since 36 Ma: Geosphere, v. 1, no. 3, p. 147–172, doi: 10.1130/GES00016.1.

Mulch, A.M., Graham, S.A., and Chamberlain, C.P., 2006, Hydrogen isotopes in Eocene river gravels and paleoelevation of the Sierra Nevada: Science, v. 313, p. 87–89, doi: 10.1126/science.1125986.

Noble, D.C., Dickinson, W.R., and Clark, M.M., 1969, Collapse caldera in the Little Walker area, Mono County, California: Geological Society of America. Special Paper, v. 121, p. 536–537.

Noble, D.C., Slemmons, D.B., Korringa, M.K., Dickinson, W.R., Al-Rawi, Y., and McKee, E.H., 1974, Eureka Valley Tuff, east-central California and adjacent Nevada: Geology, v. 2, p. 139–142, doi: 10.1130/0091-7613(1974)2<139:EVTECA>2.0.CO;2.

Noble, D.C., Korringa, M.K., Church, S.E., Bowman, H.R., Silberman, M.L., and Heropoulos, C.E., 1976, Elemental and isotopic geochemistry of nonhydrated quartz latite glasses from Eureka Valley Tuff, east-central California: Geological Society of America Bulletin, v. 87, p. 754–762, doi: 10.1130/0016-7606(1976)87<754:EAIGON>2.0.CO;2.

O'Reilly, W.O., 1984, Rock and mineral magnetism: New York, Chapman and Hall, 220 p.

Ort, M.H., 1993, Eruptive processes and caldera formation in a nested downsag-collapse caldera: Cerro Panizos, central Andes Mountains: Journal of Volcanological and Geothermal Research, v. 56, p. 221–252, doi: 10.1016/0377-0273(93)90018-M.

Palmer, H.C., and MacDonald, W.D., 1999, Anisotropy of magnetic susceptibility in relation to source vents of ignimbrites: Empirical observations: Tectonophysics, v. 307, p. 207–218, doi: 10.1016/S0040-1951(99)00126-2.

Palmer, H.C., MacDonald, W.D., and Hayatsu, A., 1991, Magnetic, structural and geochronologic evidence bearing on volcanic sources and Oligocene deformation of ash flow tuffs, northeast Nevada: Journal of Geophysical Research, v. 96, p. 2185–2202.

Palmer, H.C., MacDonald, W.D., Gromme, C.S., and Ellwood, B.B., 1996, Magnetic properties and emplacement of the Bishop Tuff, California: Bulletin of Volcanology, v. 58, p. 101–116, doi: 10.1007/s004450050129.

Piper, A.M., Gale, H.S., Thomas, H.E., and Robinson, T.W., 1939, Geology and ground-water hydrology of the Mokelumne area, California: U.S. Geological Survey Water-Supply Paper 780, 230 p.

Priest, G.R., 1979, Geology and geochemistry of the Little Walker volcanic center, Mono County, California [Ph. D. thesis]: Corvallis, Oregon, Oregon State University, 253 p.

Ransome, F.L., 1898, Some lava flows of the western slope of the Sierra Nevada, California: U.S. Geological Survey Bulletin 89, 74 p.

Rhodes, R.C., and Smith, E.I., 1972, Distribution and directional fabric of ash-flow sheets in the northwestern Mogollon Plateau, New Mexico: Geological Society of America Bulletin, v. 83, p. 1863–1868, doi: 10.1130/0016-7606(1972)83[1863:DADFOA]2.0.CO;2.

Slemmons, D.B., 1953, Geology of the Sonora Pass region [Ph.D. thesis]: Berkeley, California, University of California, 201 p.

Slemmons, D.B., 1966, Cenozoic volcanism of the central Sierra Nevada, California, *in* Bailey, E.H., ed., Geology of northern California: California Division of Mines and Geology Bulletin 190, p. 199–208.

Stewart, J.H., 1978, Basin-range structure in western North America, *in* Smith, R.B. and Eaton, G.P., eds., Cenozoic tectonics and regional geophysics of the western Cordillera: Geological Society of America Memoir 152, p. 1–32, plate 1-1.

Stewart, J.H., 1988, Tectonics of the Walker Lane Belt, western Great Basin Mesozoic and Cenozoic deformation in a zone of shear, *in* Ernst, W.G., ed., Metamorphism and crustal evolution of the western U.S.: Upper Saddle River, New Jersey, Prentice-Hall, Rubey Volume VII, p. 685–713.

Thatcher, W., Foulger, G.R., Julian, B.R., Svarc, J.L., Quilty, E., and Bawden, G.W., 1999, Present-day deformation across the Basin and Range Province, western United States: Science, v. 283, p. 1714–1717, doi: 10.1126/science.283.5408.1714.

Trask, J.B., 1856, Report on the geology of northern and southern California: Embracing the mineral and agricultural resources of those sections, with statistics of the northern, southern and middle mines: Sacramento, California, State Senate Document no. 14, Session of 1856, 66 p.

Unruh, J.R., 1991, The uplift of the Sierra Nevada and implications for Late Cenozoic epeirogeny in the western Cordillera: Geological Society of America Bulletin, v. 103, p. 1395–1404, doi: 10.1130/0016-7606(1991)103<1395:TUOTSN>2.3.CO;2.

Wagner, D.L., Jennings, C.W., Bedrossian, T.L., and Bortugno, E.J., 1987, Sacramento quadrangle map no. 1A: California Division of Mines and Geology, Regional Geological Map Series, scale 1:250,000, 4 sheets.

Wagner, D.L., Bortugno, E.J., and McJunkin, R.D., 1990, Geologic map of the San Francisco-San Jose quadrangle: California Division of Mines and Geology, Regional Geologic Map Series, scale 1:250,000, 5 sheets.

Wakabayashi, J., and Sawyer, T., 2001, Stream incision, tectonics, uplift, and evolution of topography of the Sierra Nevada, California: The Journal of Geology, v. 109, p. 539–562, doi: 10.1086/321962.

Wells, R.E., and Hillhouse, J.W., 1989, Paleomagnetism and tectonic rotation of the lower Miocene Peach Springs Tuff: Colorado Plateau, Arizona, to Barstow, California: Geological Society of America Bulletin, v. 101, p. 846–863, doi: 10.1130/0016-7606(1989)101<0846:PATROT>2.3.CO;2.

Wernicke, B., and Snow, J.K., 1998, Cenozoic tectonism in the central Basin and Range: Motion of the Sierran-Great Valley Block: International Geology Review, v. 40, p. 403–410.

Wesnousky, S.G., 2005, Active faulting in the Walker Lane: Tectonics, v. 24, p. TC3009, doi: 10.1029/2004TC001645.

Whitney, J.D., 1865, Geology: Philadelphia, Caxton Press, Geological Survey of California, v. 1, p. 243–246 (as quoted in Ransome, 1898).

Wolfe, J.A., Schorn, H.E., Forest, C.E., and Molnar, P., 1997, Paleobotanical evidence for high altitudes in Nevada during the Miocene: Science, v. 276, p. 1672–1675, doi: 10.1126/science.276.5319.1672.

Young, R.A., and Brennan, W.J., 1974, Peach Springs Tuff: Its bearing on structural evolution of the Colorado Plateau and development of Cenozoic drainage in Mohave County, Arizona: Geological Society of America Bulletin, v. 85, p. 83–90, doi: 10.1130/0016-7606(1974)85<83:PSTIBO>2.0.CO;2.

Zijderveld, J.D.A., 1967, A.C. demagnetization of rocks: Analysis of results, *in* Collinson, D.W., et al., eds., Methods of palaeomagnetism: Amsterdam, Elsevier, p. 254–286.

Manuscript Received 25 May 2007
Revised Manuscript Received 22 August 2007
Manuscript Accepted 22 August 2007